Newsletters on Stratigraphy
Published online February 2023

EarlyAccess-Article

Impact of early Danian environmental perturbations on mid-latitude planktic foraminiferal assemblages from the ODP Site 1262 (South Atlantic Ocean)

Guilherme Krahl[1,2]*, Ignacio Arenillas[3], Vicente Gilabert[3,4], Karlos G. D. Kochhann[1,2], Marlone H. H. Bom[1,2], Gerson Fauth[1,2] and José A. Arz[3]

With 9 figures

Abstract. After the mass extinction at the Cretaceous/Paleogene (K/Pg) boundary (~66 Ma), life forms quickly radiated to occupy ecological niches in the world's oceans. Nevertheless, the aftermath of the Chicxulub impact, the massive volcanism of the Deccan Traps and climatic perturbations endured during the early Danian. The impact of consequent carbon cycle perturbations on nascent plankton communities, such as the Dan-C2 event (~65.80 to ~65.71 Ma), is still poorly known. In this work, we present a detailed study of planktic foraminiferal assemblages from Ocean Drilling Program (ODP) Site 1262 (Walvis Ridge, South Atlantic Ocean), spanning the first ~400 kyr of the Danian. No relevant perturbations in planktic foraminiferal assemblages and carbonate preservation indices have been identified at Site 1262 during the Dan-C2 event. Approximately 50 kyr before the beginning of the Dan-C2 event, a Hg-rich interval, potentially linked to the emplacement of the Ambenali Formation of the Deccan Traps massive volcanism, is recorded between ~65.95 and 65.82 Ma. It coincides with an increase in aberrant planktic foraminifera (~65.93 to ~65.82 Ma), allowing to establish a cause-effect relationship. Additionally, a bloom of triserial guembelitriids was recognized between ~65.87 and ~65.78 Ma, also preceding the Dan-C2 event but lagging the Hg-rich interval and the bloom of aberrant planktic foraminifera. The lag time between the first volcanic episode and ecosystem response may be due to factors such as an inefficient biological pump and increases in temperature, microbial activity and food supply at the ocean surface. A second Hg-rich interval identified between ~65.70 and ~65.65 Ma has been tentatively tied to the Mahabaleswar Formation of the Deccan Traps. Neither the second volcanic episode nor the Dan-C2 event resulted in relevant environmental perturbations at Site 1262. This suggests that, although volcanism may have had an impact on early plankton communities in the early Danian through metal contamination, marine ecosystems likely became progressively more stable and resistant to changes in volcanic emissions and the carbon cycle.

Key words. Early Danian, planktic foraminifera, mercury, Dan-C2, Deccan Traps

Authors' addresses:
[1] Technological Institute for Paleoceanography and Climate Change, itt OCEANEON, UNISINOS University, Av. UNISINOS, 950, 93022-750 São Leopoldo, RS, Brazil
[2] Geology Graduate Program, UNISINOS University, Av. UNISINOS, 950, 93022-000 São Leopoldo, RS, Brazil
[3] Departamento de Ciencias de la Tierra, and Instituto Universitario de Investigación en Ciencias Ambientales de Aragón (IUCA), Universidad de Zaragoza, E-50009 Zaragoza, Spain
[4] Departament de Dinàmica de la Terra i de l'Oceà, Facultat de Ciències de la Terra de la Universitat de Barcelona, 08028, Barcelona, Spain
* Corresponding author: gkrahl@unisinos.br

www.borntraeger-cramer.de
DOI: 10.1127/nos/2023/0744
0078-0421/2023/0744 $ 6.75

1. Introduction

The mass extinction at the Cretaceous/Paleogene (K/Pg) boundary was one of the greatest extinction events in the Earth's geological history (see Schulte et al. 2010 and references therein). It was triggered by the impact of the Chicxulub asteroid in the Yucatan Peninsula (Hildebrand et al. 1991). Impact evidence is recorded globally in a fine airfall layer rich in siderophile elements (e. g., iridium, osmium and nickel), impact glasses (microtektites), Ni-spinels, and shocked quartz (Alvarez et al. 1980, Orth et al. 1981, Schulte et al. 2010, Ravizza and Vonderhaar 2012), as well as a thick complex clastic unit, which contains Chicxulub-impact-derived material and whose deposition was linked to impact-induced processes (earthquakes, tsunamis, submarine landslides, and debris flows) that took place within a distance of up to 1000 km from the Chicxulub impact structure (see Arz et al. 2022 for a review). Models based on the size, velocity, and angle of the impactor as well as the nature of the impact site, among other data, predict that the Chicxulub impact would have triggered severe environmental disturbances in the first months and years of the Danian, causing a global mass extinction event (e. g., Kring 2007, Schulte et al. 2010, Morgan et al. 2022) in which the planktic foraminifera underwent an extinction accounting for probably ~95 % of the Cretaceous species (see Arenillas et al. 2022, and references therein).

Another large-scale disturbance that occurred across the Cretaceous-Paleogene (K-Pg) transition was the eruption of ~500 000 km^3 of lava over a large area of present-day India known as the Deccan Traps (DT) (see Schoene et al. 2019, Sprain et al. 2019, and references therein). In order to establish the eruptive history of the DT, $^{40}Ar/^{39}Ar$ dating methods have been applied to basalt plagioclases (Sprain et al. 2019), and U–Pb dating methods to zircons collected in red bole horizons between basalt flows (Schoene et al. 2019). High-precision data from the DT show that the main phase of the eruptions started near the C30n/C29r geomagnetic polarity reversal (Maastrichtian) and diminished shortly after the C29r/C29n reversal (Danian) (Schoene et al. 2019, Sprain et al. 2019). The estimated duration of the massive volcanism of the DT is very similar in the two main eruption models proposed to date: ~700–800 kyr according to the model put forward by Schoene et al. (2019, 2021) and ~1 Myr according to that of Sprain et al. (2019). Nonetheless, there are two critical differences between the two models: 1) Schoene et al. (2019) suggest a sequence of mega-pulses, whereas Sprain et al. (2019) suggest a quasi-continuous release of lava flows; 2) according to Sprain et al. (2019), the most voluminous eruptions of the DT (i. e., those corresponding to the Poladpur, Ambenali, and Mahabaleshwar Formations) occurred in the early Danian, whereas according to Schoene et al. (2019), the eruptive pulse that originated the Poladpur Fm. occurred in the latest Maastrichtian, preceding the K/Pg mass extinction event by ~30 kyr (Schoene et al. 2019, Schoene et al. 2021). According to Sprain et al. (2019), the emplacement of the Ambelani Fm. occurred between ~65.95 and 65.62 Ma (~50 and 380 kyr after the K/Pg boundary), with a pulse between ~65.95 and 65.85 Ma (50 and 150 kyr after the K/Pg boundary) according to Schoene et al. (2019). The onset of Mahabaleshwar Fm. emplacement occurred ~65.62 Ma (380 kyr after the K/Pg boundary), with a pulse between 65.62 and 65.57 Ma (380 and 430 kyr after the K/Pg boundary) according to Schoene et al. (2019).

Between the K/Pg and C29r/C29n boundaries, the first recorded paleoclimatic event of the Danian is known as Dan-C2 (Quillévéré et al. 2008), which has been attributed to large-scale inputs of greenhouse gases from the DT (Coccioni et al. 2010, Punekar et al. 2014). The Dan-C2 event is typically recorded by a double negative carbon isotope excursion (CIE-1 and CIE-2) and lasted for ~100 kyr (Quillévéré et al. 2008, Gilabert et al. 2022). The onset of this event varies slightly with the astrochronological age model used as a reference, being estimated to occur ~160 kyr after the K/Pg boundary by Barnet et al. (2019) or 200 kyr after the K/Pg boundary by Gilabert et al. (2022). The two age models differ mainly in the astronomical solution used, but they agree in tying Dan-C2 to the first 405-kyr eccentricity maximum ($Pc_{405}1$) of the Paleocene (Barnet et al. 2019; Gilabert et al. 2022). Dan-C2 shows broad similarity to other hyperthermal events, for example negative carbon ($\delta^{13}C$) and oxygen ($\delta^{18}O$) isotope excursions measured in bulk sediments and planktic foraminifera, coupled with drops in $CaCO_3$ content in deep ocean sediments. So far, the record of this event is restricted to the following Atlantic and Tethyan localities: Ocean Drilling Program (ODP) Site 1049C (NW Atlantic; Quillévéré et al. 2008), Deep Sea Drilling Program (DSDP) Sites 527 and 528 (SE Atlantic; Quillévéré et al. 2008), ODP Site 1262 (SE Atlantic; Kroon et al. 2007, Barnet et al. 2019),

Gubbio (Italy; Coccioni et al. 2010), DSDP Site 516F (SE Atlantic; Krahl et al. 2020), Caravaca (SE Spain; Gilabert et al. 2021), and Zumaia (N Spain; Gilabert et al. 2022).

In general, hyperthermal events are paced and modulated by astronomical frequencies, specifically by eccentricity (see Westerhold et al. 2020, and references therein). Bottom-water oxygenation (ventilation) decreased in the deep Atlantic Ocean (Coccioni et al. 2010, Krahl et al. 2020), and a ~4 °C warming in North Atlantic surface waters occurred during the Dan-C2 event (Quillévéré et al. 2008). However, in contrast to other hyperthermal events, no warming in deep waters (e. g., $\delta^{18}O_{benthic}$) has yet been recorded for Dan-C2 (Quillévéré et al. 2008, Barnet et al. 2019, Arreguín-Rodríguez et al. 2021), raising the question as to whether it was indeed a hyperthermal event (Barnet et al. 2019).

Planktic foraminifera and calcareous nannofossils were strongly affected by the K/Pg boundary extinction event (e. g., Smit 1982, Molina et al. 1996, Olsson et al. 1999, Arenillas et al. 2000ab, Thibault et al. 2016, Lowery et al. 2018). The high rates of species-level extinction reduced the richness of phyto- and zooplankton communities, affecting several trophic levels in the ocean (Sheehan et al. 1996). The early Danian was a time of ecosystem recovery after the K/Pg boundary extinction (Molina 2015). The earliest Danian assemblages are characterized by low diversity, high single-species dominance, and rapid evolutionary turnovers (Smit 1982, Arenillas et al. 2000a, Aze et al. 2011, Arenillas and Arz 2017, Huber et al. 2020, Lowery et al. 2021), as well as by blooms of smaller generalist and/or opportunist species (Kroon and Nederbragt 1990, Arenillas et al. 2000b, Pardo and Keller 2008, Punekar et al. 2014, Gilabert et al. 2021). During the recovery of species richness in the early Danian (Lowery and Fraass 2019), planktic foraminifera also responded to carbon cycle perturbations (e. g., Jehle et al. 2015, Jehle et al. 2019, Bornemann et al. 2021). However, the impact of Dan-C2 and the influence of the DT eruptions on early Danian planktic foraminiferal assemblages is poorly understood (Gilabert et al. 2021, Gilabert et al. 2022).

Here we present a multiproxy approach to investigate the impact of DT volcanism and the Dan-C2 event on early Danian planktic foraminiferal assemblages in the South Atlantic Ocean. We studied the lower Danian interval at Ocean Drilling Program (ODP) Site 1262, drilled on the Walvis Ridge, which presents an excellent record of the Dan-C2 event (Zachos et al. 2004). Site 1262 has been the basis for several multiproxy studies exploring carbon cycle dynamics (e. g., Birch et al. 2016, Birch et al. 2021, Woelders et al. 2017, Hull et al. 2020), as well as for the characterization of the Dan-C2 event (e. g., Barnet et al. 2019, Arreguín-Rodríguez et al. 2021). Together with other well-known localities, it has allowed the astronomical calibration of the Danian events (Dinarès-Turell et al. 2014) upon which the Geological Time Scale GTS2020 for the Danian is based (Gradstein et al. 2020).

2. Material and methods

2.1. Geographical location and stratigraphy of Site 1262

During ODP Leg 208, Sites 1262 and 1267 cored the K–Pg transition on the Walvis Ridge, eastern South Atlantic Ocean (27°11.15′ S, 1°34.62′ W; Zachos et al. 2004). We studied Hole 1262B by collecting forty samples across the K-Pg transition of core 208-1262B-22H-3-5 (Fig. 1), which was located at a paleolatitude of ~40° S (Van Hinsbergen et al. 2015) and deposited in the upper abyssal zone (~3000 m water depth; Zachos et al. 2004). The depths assigned to each sample correspond with the meters composite depth scale (mcd), spanning the interval between 216.83 and 214.88 mcd. Overall, the sediments recovered at Site 1262 vary from clays to carbonate-rich oozes (Zachos et al. 2004).

The K/Pg boundary (208-1262B-22H-4, 137 cm; 216.52 mcd) is marked by an irregular contact between upper Maastrichtian light gray-brown clayey nannofossil oozes and overlying lower Danian red-brown clays (Fig. 2; see Appendix A), the latter of which are moderately bioturbated. Microtektites (impact glasses) related to the Chicxulub impact have been reported within this reddish clay directly above the K/Pg boundary (Zachos et al. 2004). The magnetostratigraphy of Site 1262 is based on shipboard paleomagnetic measurements conducted at 5-cm resolution, supplemented by discrete samples (Bowles 2006, Westerhold et al. 2008). On this basis, the C29r/C29n reversal was placed at 215.00 mcd (Bowles 2006, Westerhold et al. 2008, Dinarès-Turell et al. 2014). Complementary to these findings, Site 1262 has been the subject of several studies reporting sedimentological and geochemical

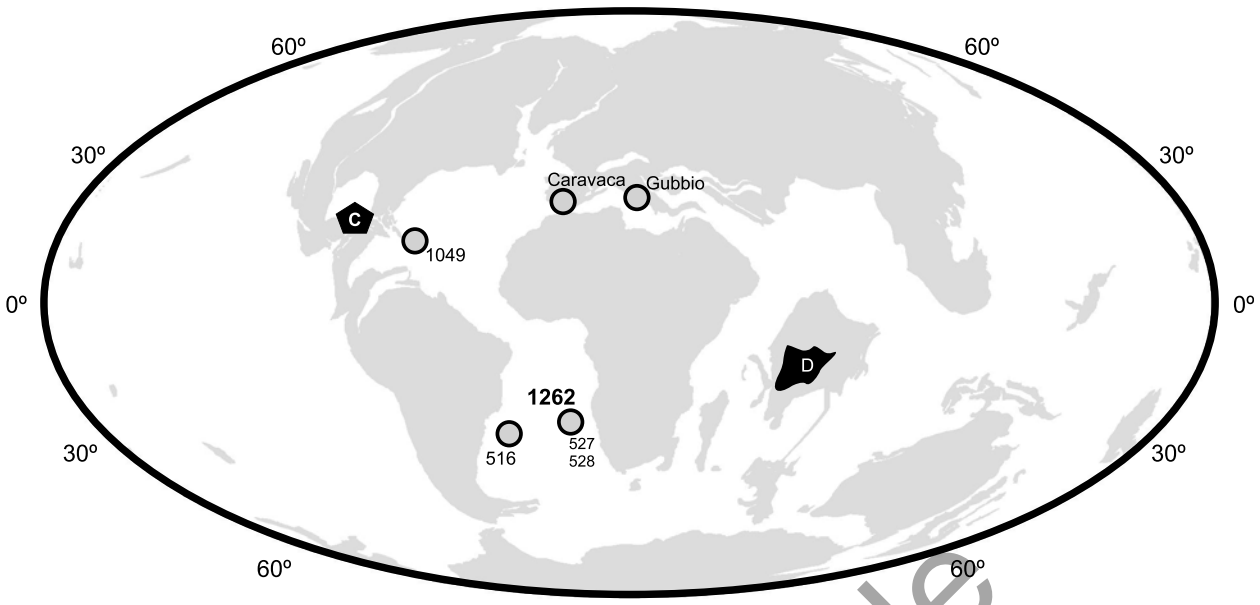

Fig. 1. Paleogeographic reconstruction for the K/Pg boundary (66 Ma) after ODSN plate reconstruction (ODSN system: http://www.odsn.de/odsn/services/paleomap/paleomap.html), showing the location of ODP Site 1262 and other localities discussed in the text. Abbreviations: C = Chicxulub crater; D = Deccan Traps.

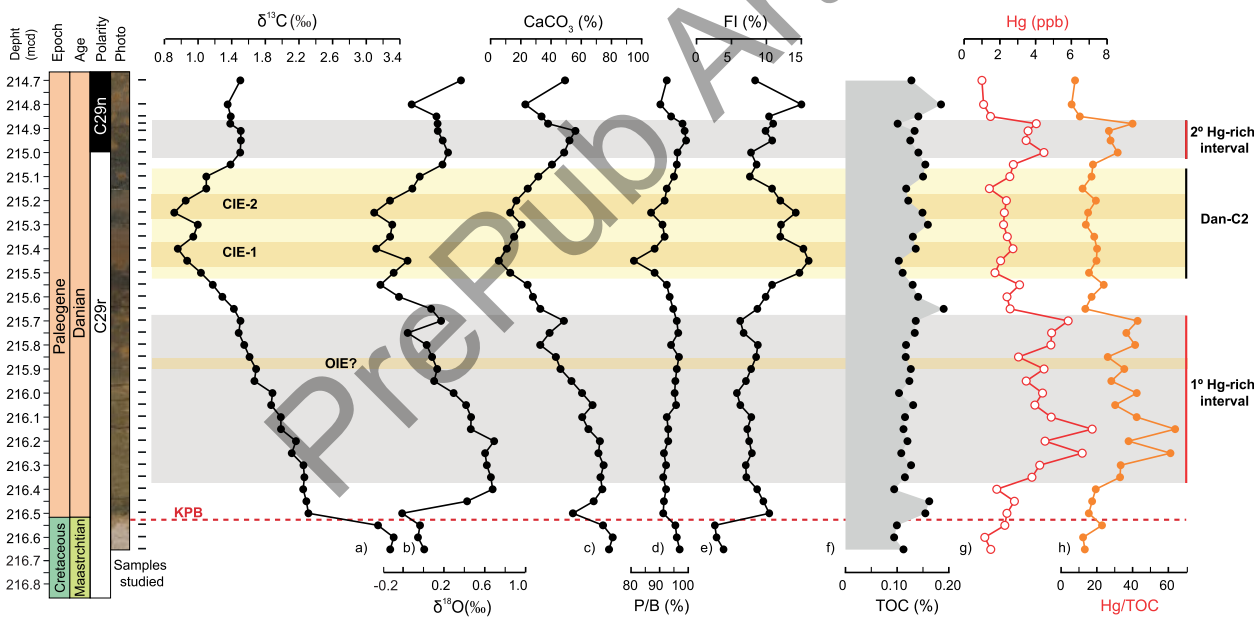

Fig. 2. Geochemical record at Site 1262. a) bulk sediment carbon ($\delta^{13}C$, ‰); b) oxygen stable isotopes ($\delta^{18}O$, ‰); c) calcium carbonate content ($CaCO_3$ %); d) planktic/benthic foraminiferal ratio: P/B ratio (%); e) foraminiferal fragmentation index: FI (%); f) total organic carbon (TOC) content; g) Hg concentration (ppb) and Hg/TOC ratio. Stratigraphic position of the C29r/C29r reversal at Hole B according to Bowles (2006) and Westerhold et al. (2008). Stratigraphic position of CIE-1 and CIE-2 od Dan-C2 based on this study. Estimated stratigraphic position of oxygen isotope excursion (OIE) based on the correlation with Hole C (see Appendix A). KPB = Cretaceous/Paleogene boundary.

data (such as oxygen, carbon, and osmium isotopes) for the studied interval (e. g., Ravizza and Peucker-Ehrenbrink 2003, Robinson et al. 2009, Kroon et al. 2007, Alegret et al. 2012, Birch et al. 2016, Woelders et al. 2017, Barnet et al. 2018, Barnet et al. 2019, Hull et al. 2020).

2.2. Micropaleontological methods and the planktic foraminiferal dataset

For each sample collected from Site 1262, approximately 10 g of sediments were soaked in deionized water for 72 hours, before being washed over 63 µm sieves. The residues were dried in an oven at temperatures below 40 °C. We picked approximately 400 planktic foraminiferal specimens per sample from the ≥63 µm residues. The quantitative planktic foraminiferal distribution and paleoenvironmental indexes at Site 1262 are shown in Appendix B, and the depth habitats of the planktic foraminiferal species in Appendix C. Taxonomic identifications at genus and species levels followed Olsson et al. (1999) and Koutsoukos (2014), whereas biostratigraphic interpretations are based on Berggren and Pearson (2005) and Wade et al. (2011). For comparison, we have also used the most recent biozonation of Arenillas et al. (2021) for the lower Danian, which is based on the taxonomic and biostratigraphic interpretations of Arenillas et al. (2000a, 2000b, 2004, 2018). In light of the known paleoecological preferences of the identified taxa (Boersma and Premoli Silva 1983, D'Hondt and Zachos 1993, Huber and Boersma 1994, Berggren and Norris 1997, Olsson et al. 1999, Coxall et al. 2000, Aze et al. 2011, Koutsoukos 2014, Huber et al. 2020), we grouped them according to their inferred paleodepth habitats into ecogroups (mixed-layer, thermocline and sub-thermocline taxa; see Appendix C). Variations in the relative abundances of these groups are useful to evaluate changes in water column stratification (e. g., Lowery et al. 2021).

Changes in the relative abundances of planktic and benthic foraminifera (the P/B ratio) may be related to paleobathymetry (e. g., Van der Zwaan et al. 1990), paleoproductivity (e. g., Berger and Diester-Haass 1988), and/or carbonate dissolution at the seafloor (e. g., Hancock and Dickens 2005, Nguyen and Speijer 2014, Luciani et al. 2017). Given that the paleobathymetry at Site 1262 did not change markedly within the studied interval (Zachos et al. 2004), we assume that changes in the P/B ratio were mainly caused by changes in the calcite saturation state of deep waters and, to a lesser extent, by changes in paleoproductivity. We calculated the P/B ratio as follows: P/B ratio (%) = [planktic specimens/(planktic + benthic specimens) *100].

We also calculated the fragmentation index (FI) quantifying the number of fragmented individuals. We counted as fragments specimens with clearly missing or deteriorated chambers, as well as specimens exhibiting features of fragmentation such as large holes. The fragmentation index was calculated as follows: FI (%) = [(number of fragments)/(number of fragments + complete individuals) *100].

Finally, we estimated the foraminiferal abnormality index (FAI) in accordance with the morphological criteria used by Arenillas et al. (2018). To identify morphological abnormalities in foraminiferal tests, we compared forms considered aberrant with typical "normal" specimens recognized in the literature (e. g., Olsson et al. 1999, Arenillas et al. 2018, Arenillas et al. 2021).

2.3. Geochemical methods (stable isotopes, carbonate content, Hg and Mn content)

Approximately 1.5 g of bulk sediments from each sample were crushed with an agate mortar and pestle for stable isotope analysis. Sample aliquots (100–150 µg) were reacted with phosphoric acid, and the resulting CO_2 was analyzed with a Finnigan MAT 253 mass spectrometer coupled to a Carbo-Kiel type IV device at the Leibniz Laboratory for Radiometric Dating and Stable Isotope Research, University of Kiel. The standard external error based on duplicate measurements is better than ±0.05‰ for $\delta^{13}C_{bulk}$ and ±0.08‰ for $\delta^{18}O_{bulk}$. The results were calibrated against the standard NBS-19, and values are reported as deviations (‰) from the Vienna PeeDee Belemnite scale (VPDB).

The carbonate content ($CaCO_3$%) was measured in oven-dried (38–40 ºC for 48 hours) ground sediment samples from Site 1262. For each sample, a ~0.26 g aliquot of homogenized sediments was measured for total carbon (TC) content in a LECO SC-144DR carbon and sulfur analyzer at the Technological Institute for Paleoceanography and Climate Change (itt OCEANEON; UNISINOS University). Total organic carbon (TOC) was also measured in ~0.26 g sample aliquots after the sediments had been treated with HCl 6N and washed with warm water until neutral pH (pH = 7) was reached. We calculated the $CaCO_3$ content according to Stax and Stein (1995) as follows: $CaCO_3$% = [TC(%) – TOC(%)] * 8.33. Since our primary goals were to analyze the planktic foraminiferal assemblages and measure the Hg and Mn content of the samples in order to assess the DT volcanism at Site 1262 (see just below), the sampling resolution for isotopic analysis is markedly lower than that of Woelders et al. (2017), so we have compared and

correlated the $\delta^{13}C_{bulk}$ and $\delta^{18}O_{bulk}$ data of these authors in Appendix A. Geochemical data from Site 1262 are shown in Appendix D.

For determination of mercury (Hg) concentrations were measured (~0.5 to 0.7 g of bulk sediment aliquots) by an atomic absorption using a direct mercury analyzer (Milestone- DMA-80 evo Tricell) in the itt Oceaneon (Universidade do Vale do Rio dos Sinos). All 40 samples is initially dried and thermally decomposed in an oxygen flow, where the Hg vapors are trapped on a gold amalgamator and subsequently desorbed for quantification. Finally, the Hg content is determined using atomic absorption spectrophotometry (253.65 nm). Mn concentrations were measured for the same set of samples after digestion of 150 mg per g of ground sediments in a solution of nitric and hydrochloric acids, using an inductively coupled plasma optical emission spectroscope (ICP-OES) iCAP 7400 (Thermo Fischer Scientific). Both analyses were carried out at itt OCEANEON (UNISINOS University).

3. Results

3.1. Record of CIEs and carbonate preservation disturbances at Site 1262

The $\delta^{13}C_{bulk}$ record at Hole 1262B (Fig. 2a, b) displays the negative isotope excursion usually associated with the K/Pg boundary (~1‰ $\delta^{13}C$) between the samples at 216.55 and 216.50 mcd and the Dan-C2 double-peaked negative excursion between 215.52 and 215.07 mcd. According to our $\delta^{13}C_{bulk}$ data, the CIE-1 of the Dan-C2 event (lowest $\delta^{13}C$) is placed between 215.47 and 215.37 mcd, and the CIE-2 of Dan-C2 between 215.27 and 215.17 mcd (Fig. 2). Our isotope data show a similar behaviour as those from Hole 1262C previously reported by Woelders et al. (2017), albeit of lower resolution. Unlike our isotope data from Hole 1262B, Woelders et al. (2017) identified a negative $\delta^{18}O_{bulk}$ excursion at ~216 mcd in Hole 1262C. According to the stratigraphic correlation in Appendix A, this oxygen isotope excursion should be placed approximately between 215.92 and 215.86 mcd in Hole 1262B. From this horizon onwards, the $\delta^{18}O_{bulk}$ values remain relatively high until the top of the Dan-C2 interval.

The carbonate content appears to oscillate parallel to $\delta^{13}C_{bulk}$ and $\delta^{18}O_{bulk}$, with marked drops at the K/Pg boundary (from 74.41 to 54.47 %) and within the Dan-C2 interval (decreasing to approximately 20 %; Fig. 2c). We recognize a third drop in $CaCO_3$ content (from 56.13 to 23 %) and $\delta^{18}O_{bulk}$ centered at 214.80 mcd, although this does not correlate with a CIE at Site 1262 (Fig. 2a). A remarkable feature of the geochemical record of Site 1262 is the progressive decline in $\delta^{13}C_{bulk}$ values and carbonate content between the K/Pg boundary and the base of the Dan-C2 interval (Fig. 2a, c).

The P/B ratio indicates a predominance of planktic foraminifera, with an average value of 93.4 % across the studied interval (Fig. 2d), which is a result expected for open marine conditions and abyssal depths. Nevertheless, the P/B ratio drops to 81.0 % at the base of the Dan-C2 interval, rapidly recovering before the first CIE. The average value of the fragmentation index (FI) across the studied section is 9.14 % (Fig. 2e). Although this average FI value is low, it is noteworthy that, between 215.55 and 215.15 mcd, the FI reaches a mean value of 13.4 %, the highest in the whole dataset (Appendix B). The FI value rises sporadically at 214.80 mcd, reaching an isolated maximum of 15.0 %. This rise in FI coincides with the decrease in $CaCO_3$ content (33.69 to 23 %) and a drop in the $\delta^{18}O_{bulk}$ value (0.127 to –0.116‰) (Fig. 2a), as well as a moderate decrease in the P/B ratio (94 to 90.25 %) (Fig. 2d).

3.2. Mercury chemostratigraphy

Hg concentrations in sediment measured at Site 1262 varied between 0.99 and 7.16 ppb, with an average of 3.19 ppb. Two intervals of increased Hg concentration were observed during the lower Danian (Fig. 2g). The first interval, between 216.37 and 215.67 mcd, exhibits Hg concentrations ranging from 3.04 to 7.16 ppb (average = 4.72 ppb). In the second interval (215.02 to 214.86 mcd), the Hg concentrations show a mean value of 3.88 ppb (max. = 4.46 ppb). It is noteworthy that the Hg concentrations remain low in the interval assigned to the Dan-C2 event. Within the Dan-C2 interval, the Hg concentrations range between 2.41 and 1.41 ppb (averaging 2.66 ppb) (Fig. 2g).

The Hg/TOC ratio (Fig. 2h) depicts trends similar to the values of the Hg concentrations. Two positive Hg/TOC anomalies can be recognized: (i) between 216.37 and 215.67 mcd (average = 39.58; max. = 63.80; min. = 26.09), and (ii) between 215.02 to 214.86 mcd (average = 31.51; max. = 39.98; min. = 27.66). Within the Dan-C2 interval, the Hg/TOC ratio remains low (Fig. 2h), at between 20.11 and 12.02 (average = 16.98). At Site 1262 (Fig. 2 g, h), the base (215.02 mcd) of the second Hg and Hg/TOC anomaly

(ii) is located slightly below the top of the CIE-2 of the Dan-C2 interval (215.17 mcd).

3.3. Planktic foraminiferal biostratigraphy

To study the planktic foraminiferal biostratigraphy and assemblages at Site 1262, we used a sampling resolution of between 3 and 5 cm. In the lower Danian of Site 1262, we recognized eighteen planktic foraminiferal species, which were assigned to seven genera according to the taxonomy of Olsson et al. (1999) and Koutsoukos (2014) (Appendix B). Through the text and figures, moreover, we show the equivalence of this taxonomy to the more splitter-oriented taxonomy of Arenillas et al. (2021, and references therein). Most of the Danian species identified at Site 1262 are illustrated in Figs 3 and 4. Changes in the relative abundance of the Danian planktic foraminiferal species at Site 1262 are illustrated in Fig. 5.

The highest occurrences (HOs) of typical Cretaceous species, assigned to the genera Abathomphalus, Globotruncana, Globotruncanita, Contusotruncana, Heterohelix s. l. (Planoheterohelix and Laeviheterohelix), Pseudoguembelina, Pseudotextularia, Planoglobulina, Racemiguembelina, Rugoglobigerina, Muricohedbergella, Planohedbergella and Globigerinelloides, were identified at 216.55 mcd, characterizing the uppermost part of the Pseudoguembelina hariaensis Zone sensu Nederbragt (1991). Some Cretaceous planktic foraminiferal specimens were observed in small proportions in the lowermost Danian samples and have been interpreted as reworked.

The lower Danian key-biohorizons recognized at Site 1262 were the lowest occurrence (LO) of *Parasubbotina pseudobulloides* at 216.32 mcd (Fig. 5q, Appendix B), the HO of *Parvularugoglobigerina eugubina* s. l. (*Trochoguembelitria*, i. e., trochospiral guembelitriids with a pore-mounded, rugose wall) at 216.17 mcd (Fig. 5g, Appendix B), and the LO of *Subbotina triloculinoides* at 215.82 mcd (Fig. 5r, Appendix B). This stratigraphic interval corresponds to Subbiozones Dan3b, Dan4c and Dan4b of Arenillas et al. (2021), suggesting a small hiatus that affects the lowermost Danian, probably Biozone P0 (or Dan1) and the lower part of Biozone Pα (Dan2 and Dan3a). Nevertheless, this hiatus could be even smaller if there is condensed sedimentation between the uppermost Maastrichtian sample and the lowermost Danian sample studied here, where Chicxulub-impact-derived microtektites have been identified (see section 4.1).

3.4. Planktic foraminiferal assemblages after the K/Pg boundary

The composition and structure of planktic foraminiferal assemblages at Site 1262 were modified significantly during the earliest Danian (Figs 5 and 6). The relative abundance of microperforated species for the whole interval was 47.4 %, with relative abundances ranging between 31.0 % and 87.5 % (Fig. 6a). These species belong to the families Guembelitriidae (genera *Guembelitria* s. l. [*Chiloguembelitria*], *Globoconusa* and *Parvularugoglobigerina* s. l. [*Trochoguembelitria*]) and Chiloguembelinidae (genera *Woodringina* and *Chiloguembelina*) (Fig. 5a to 5h). The relative abundance of normally perforated taxa for the whole interval was 52.5 %, ranging between 12.5 and 69 %. Species with normal perforations belong to the families Eoglobigerinidae (genera *Eoglobigerina*, *Parasubbotina*, and *Subbotina*), Truncorotaloididae (genus *Praemurica*), and Globanomalidae (genus *Globanomalina*) (Figs 5i to 5r).

In the first 25 cm (up to 216.27 mcd) above the K/Pg boundary, an increase in species richness is observed (Fig. 5s). The test size of the species identified in this stratigraphic interval (Fig. 6 sample B) is considerably smaller than those in the Maastrichtian (Fig. 6, sample A). This interval is characterized by increased abundances of microperforated species (Fig. 6a), represented mainly by species of *Woodringina* and *Guembelitria* s. l. (*Chiloguembelitria*) (Figs 5a to 5c). The relative abundance of mixed-layer species, which include the microperforate species and those of *Praemurica*, is also very high (75.1 %), whereas thermocline and sub-thermocline species are predominant above this interval (Fig. 6b).

Guembelitria s. l. [*Chiloguembelitria*] increases in relative abundance between 215.92 and 215.12 mcd, with a bloom between 215.97 and 215.42 mcd. Therefore, at Site 1262, the bloom of triserial guembelitriids is first recorded 40 cm below the base of the Dan-C2 interval at 215.52 mcd (Fig. 6), but the relative abundance of *Guembelitria* s. l. remains relatively high until almost the top of the Dan-C2 interval at 215.17 mcd (Fig. 6). There is also a small increase in the FAI between 216.27 and 215.62 mcd (1.37 %), with two pronounced peaks at 216.1 (1.75 %) and 215.8 mcd (2.6 %) (Fig. 6d). Although the relative abundances of aberrant specimens are overall low (~2 %), they exceed background levels between 216.27 and 215.67 mcd. The specimens with aberrant tests mostly belong to the families Truncorotaloididae

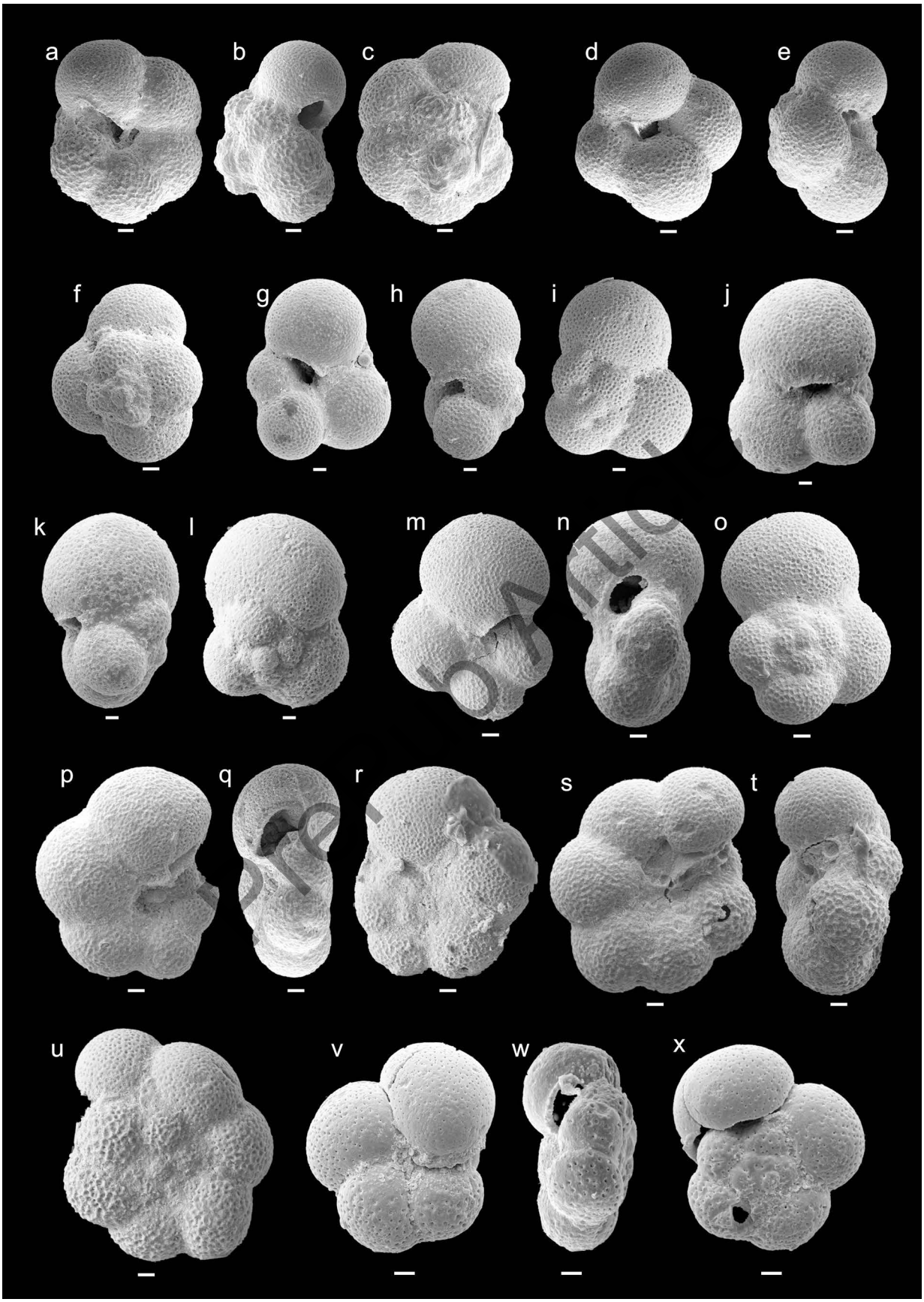
a
b
c
d
e
f
g
h
i
j
k
l
m
n
o
p
q
r
s
t
u
v
w
x

Fig. 3. Scanning electron microscope (SEM) micrographs of Danian planktic foraminifera from Site 1262 (scale bars = 10 μm). a–c. *Eoglobigerina edita* (*E. polycamera* according to A21) (215.78 mcd). d–f. *Eoglobigerina eobulloides* (*E.* cf. *trivialis* according to A21) (215.43 mcd). g–i. *Subbotina trivialis* (*E.* cf. *trivialis* according to A21) (215.29 mcd). j–l. *Subbotina triloculinoides* (214.88 mcd). m–o. *Parasubbotina varianta* (214.88 mcd). p–r. *Praemurica pseudoinconstans* (215.10 mcd). s–u. *Praemurica taurica* (215.89 mcd). v–x. *Globanomalina planocompressa* (*G. imitata* according to A21) (215.58 mcd). A21 = Taxonomy in Arenillas et al. (2021, and references herein).

(genus *Praemurica*) and Eoglobigerinidae (genera *Subbotina*, *Parasubbotina* and *Eoglobigerina*). The abnormalities identified in these specimens were: (i) protuberant chambers (Figs 7a–b); (ii) additional chambers (Figs 7c–f); (iii) abnormal last chambers (Figs 7g–j); (iv) elongated last chambers (Figs 7k–l); (v) atypical test growth rates (Figs 7m–p). This increase in FAI is located below the double CIE interval that characterizes the Dan-C2 event.

Between the top of the Dan-C2 interval (215.17 mcd) and the C29r/C29n boundary (215 mcd) the average relative abundance of *Subbotina* increases up-core (from 5.97 % to 15.35 % in average). Similarly, *Chiloguembelina* increases its relative abundance from 6.62 % to 10.77 % (Fig. 6e). This increase in the relative abundance of *Subbotina* and *Chiloguembelina* occurs parallel to an increase in the overall planktic foraminiferal test sizes (Fig. 6, sample D). The relative abundance of these genera undergoes a sharp decrease at 214.80 mcd before returning to the overall increasing trend. This shift is possibly related to a drop in the carbonate saturation state and the consequent poorer preservation of the foraminiferal tests (Fig. 6).

4. Discussions

4.1. Age model and dating of planktic foraminiferal and isotope events

For the age model, we followed the astrochronological models reported by Dinarès-Turell et al. (2014) and Woelders et al. (2017) and the magnetostratigraphic study carried out by Bowles (2006) and Westerhold et al. (2008) at Site 1262. We chose the 405-kyr eccentricity-based tuning (Batenburg et al. 2018) because it is the most reliable for ages older than ~52 Ma (Laskar et al. 2011). Based on this astronomical framework, the age of the K/Pg boundary was calibrated at 66 001 Ma and the C29r/C29n boundary at 65 700 Ma (Dinarès-Turell et al. 2014, Gradstein et al. 2020, see Appendix E). Previous astrochronologically calibrated age models for Site 1262 (e. g., Westerhold et al. 2008, Dinarès-Turell et al. 2014, Woelders et al. 2017) used a composite depth scale for Site 1262 following the splice-tie points established by Zachos et al. (2004), which allowed correlation and combination of the Holes A, B and C of Site 1262. As we have only studied Hole B, we show the stratigraphic correlation with Hole C (Appendix A and E). The age of each sample from Hole 1262B was estimated by interpolation between the astronomically calibrated tie-points (Appendix E). Moreover, this age model was revised by taking into account the recent astronomical calibration of LOs of the earliest Danian planktic foraminiferal species (Appendix E) by Gilabert et al. (2022) from the well-known Zumaia section (Spain), which was also part of the astrochronological framework of Dinarès-Turell et al. (2014). According to our new planktic foraminiferal biostratigraphic data from Site 1262 (Fig. 5), the LOs of *Eoglobigerina* (base of Subbiozone Dan3b), *Parasubbotina*, *Globanomalina*, and *Praemurica* coincide with the lowermost Danian sample studied here (216.50 mcd), suggesting a small hiatus which possibly affects Biozone P0 (or Dan1) and the lower part of Biozone Pα (Dan2 and Dan3a). In fact, Biozone P0, according to the original definition of Smit (1982) at Caravaca (Spain; see Arenillas et al. 2021), has not been observed in any deep-sea drilling sites, including the most complete ones known to date, such as ODP Site 1049 (Blake Nose Plateau; Norris et al. 1999). Biozone P0 (or Dan1) has only been identified in the most continuous, complete and expanded lower Danian sections worldwide (Molina et al. 2009, Arenillas et al. 2021), such as El Kef and Aïn Settara (Tunisia), and Caravaca and Zumaia (Spain), which were used to establish the highest-resolution planktic foraminiferal zonations for this interval (Smit 1982, Arenillas et al. 2004, Arenillas et al. 2021).

The lowermost Danian sample studied here (216.50 mcd), where the LO of *Eoglobigerina* is recognized, has been dated to 65 975 Ma following the astronomically refined timescale of Gilabert et al. (2022), suggesting that the small hiatus could comprise the first 26 kyr of the early Danian. Nonetheless, it should be borne in mind that this sample is 2 cm above

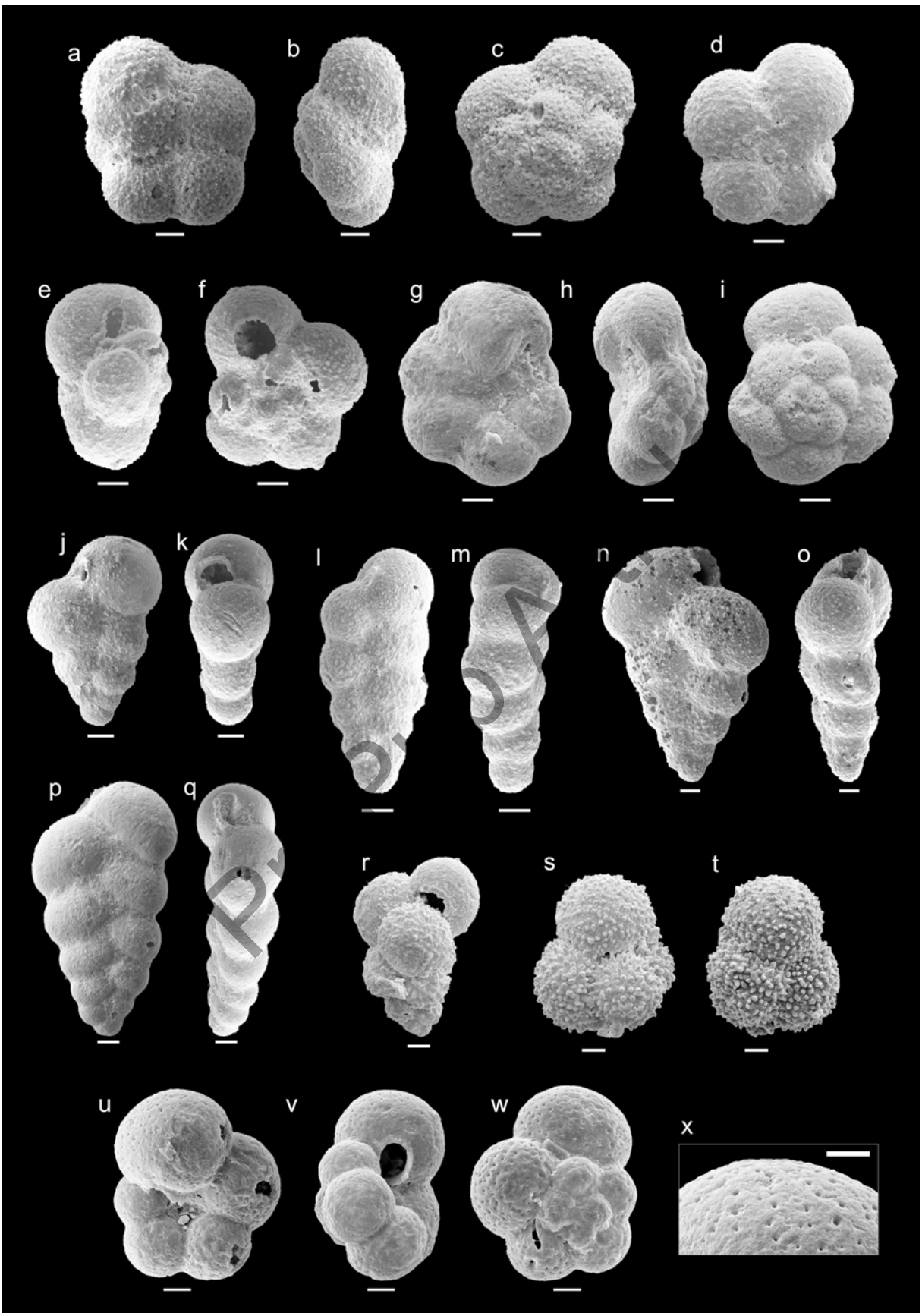

Fig. 4. SEM micrographs of Danian planktic foraminifera from Site 1262 (scale bars = 10 μm). a–c. *Praemurica nikolasi* (*Globanomalina imitata* according to A21) (215.03 mcd). d–f. *Parvularugoglobigerina eugubina* s. l. (*Trochoguembelitria liuae* according to A21) (216.03 mcd). g–i. Transitional specimen between *Parvularugoglobigerina eugubina* s. s. and *Globanomalina archaeocompressa* (large *Pv. eugubina sensu* Smit 1982) (216.63 mcd). j–k. *Woodringina claytonensis* (215.43 mcd). l–m. *Woodringina hornerstownensis* (215.07 mcd). n-o. *Chiloguembelina midwayensis* (214.88 mcd). p–q. *Chiloguembelina morsei* (*Ch. taurica* according to A21) (215.03 mcd). r. *Guembelitria cretacea* s. l. (*Chiloguembelitria danica* according to A21) (216.03 mcd). s–t. *Globoconusa daubjgersensis* (214.88 mcd). u–w. *Parasubbotina* aff. *pseudobulloides* (*Eoglobigerina praeedita* according to A21) (215.73 mcd). x. Texture detail of the latter. A21 = Taxonomy in Arenillas et al. (2021, and references herein).

the K/Pg boundary (216.52 mcd), and in this 2 cm thick basal Danian interval, Chicxulub-impact-derived microtektites and a remarkable negative $\delta^{13}C_{bulk}$ excursion have been reported (Zachos et al. 2004, Kroon et al. 2007, Woelders et al. 2017). Accordingly, Biozone P0 (Dan1) and/or the lower part of Biozone Pα (Dan2 and Dan3a) could perhaps be condensed and mixed in this basal Danian interval. For this reason, we conservatively suggest that the lowermost Danian hiatus spans roughly one precession cycle (~21 kyr). In addition, the lower Danian at Site 1262 is characterized by clays that are moderately bioturbated (Zachos et al. 2004), so the early Danian planktic foraminiferal assemblages could be mixed in the first lower Danian samples. This hypothesis could also explain why the latter contain a relatively high abundance of triserial guembelitriids, typical precisely of the absent Biozone P0 (or Dan1) and the lowermost part of Biozone Pα (or lower Dan2) (Smit 1982, Arenillas et al. 2000a, Arenillas et al. 2000b, Arenillas et al. 2018, Gilabert et al. 2021, Gilabert et al. 2022). The recognition of this small hiatus at Site 1262 precludes analysis of the evolution of planktic foraminiferal assemblages immediately after the K/Pg boundary extinction event. Furthermore, it makes it necessary to modify slightly the age model proposed by Dinarès-Turell et al. (2014) at Site 1262 (Appendix E). However, the remaining stratigraphic record studied here, i. e., from the upper part of Biozone Pα (Dan3b) to Biozone P1b (Dan4b), seems to be continuous and complete at Site 1262, allowing the Dan-C2 event to be analyzed and its relationship with DT volcanism assessed.

According to the slightly readjusted age model for Site 1262, the key biohorizons, i. e., the LO of *P. pseudobulloides* (base of Dan4), the HO of *Trochoguembelitria* (= HO of *Parvularugoglobigerina eugubina* s. l. *sensu* Olsson et al. 1999; top of Pα), and the LO of *S. triloculinoides* (bases of Biozones P1b and Dan4b), are calibrated respectively at 65.943, 65.916 and 65.854 Ma, i. e., 58, 85 and 147 kyr after the K/Pg boundary (Fig. 8). These dating are similar to those astronomically estimated by Gilabert et al. (2022), except for the LO of *S. triloculinoides*. The latter is a problematic datum because it has been placed in different stratigraphic positions: within magnetozone C29n well above Dan-C2 (Berggren and Pearson 2005, Quillévéré et al. 2008, Coccioni et al. 2010, Wade et al. 2011), at the base of C29n (Huber and Quillévéré 2005), and within magnetozone C29r (Arenillas et al. 2004, Arenillas et al. 2021), either within the Dan-C2 interval (Gilabert et al. 2021, Gilabert et al. 2022) or below the base of the Dan-C2 interval (Krahl et al. 2020, this study, Fig. 5r). These data suggest that it is a diachronous biozone marker, at least in the South Atlantic Ocean. An alternative explanation may be the taxonomic difficulties in distinguishing *S. triloculinoides* and its ancestor *Eoglobigerina microcellulosa* (see Arenillas et al. 2021), whose interspecific boundaries may be very diffuse.

According to the age model explained above the base and top of the Dan-C2 interval are calibrated at 65.798 (215.52 mcd) and 65.714 Ma (215.07 mcd), i. e., 203 and 287 kyr after the K/Pg boundary (Fig. 8a, Appendix D), which is compatible with the ages given by other authors (Barnet et al. 2019, Gilabert et al. 2022). The base and top of the CIE-1 of Dan-C2 are calibrated at 65.789 (215.47 mcd) and 65.772 Ma (215.37 mcd), i. e., 212 and 229 kyr after the K/Pg boundary. Finally, the base and top of the CIE-2 of Dan-C2 are calibrated at 65.753 (215.27 mcd) and 65.734 Ma (215.17 mcd), i. e., 248 and 267 kyr after the K/Pg boundary.

4.2. Evaluation of the carbonate preservation and Hg concentrations at Site 1262

The decreased carbonate content of the deep ocean sediments deposited during the negative CIEs of the Paleogene are usually attributed to the lysocline and carbonate compensation depth (CCD) shoaling during

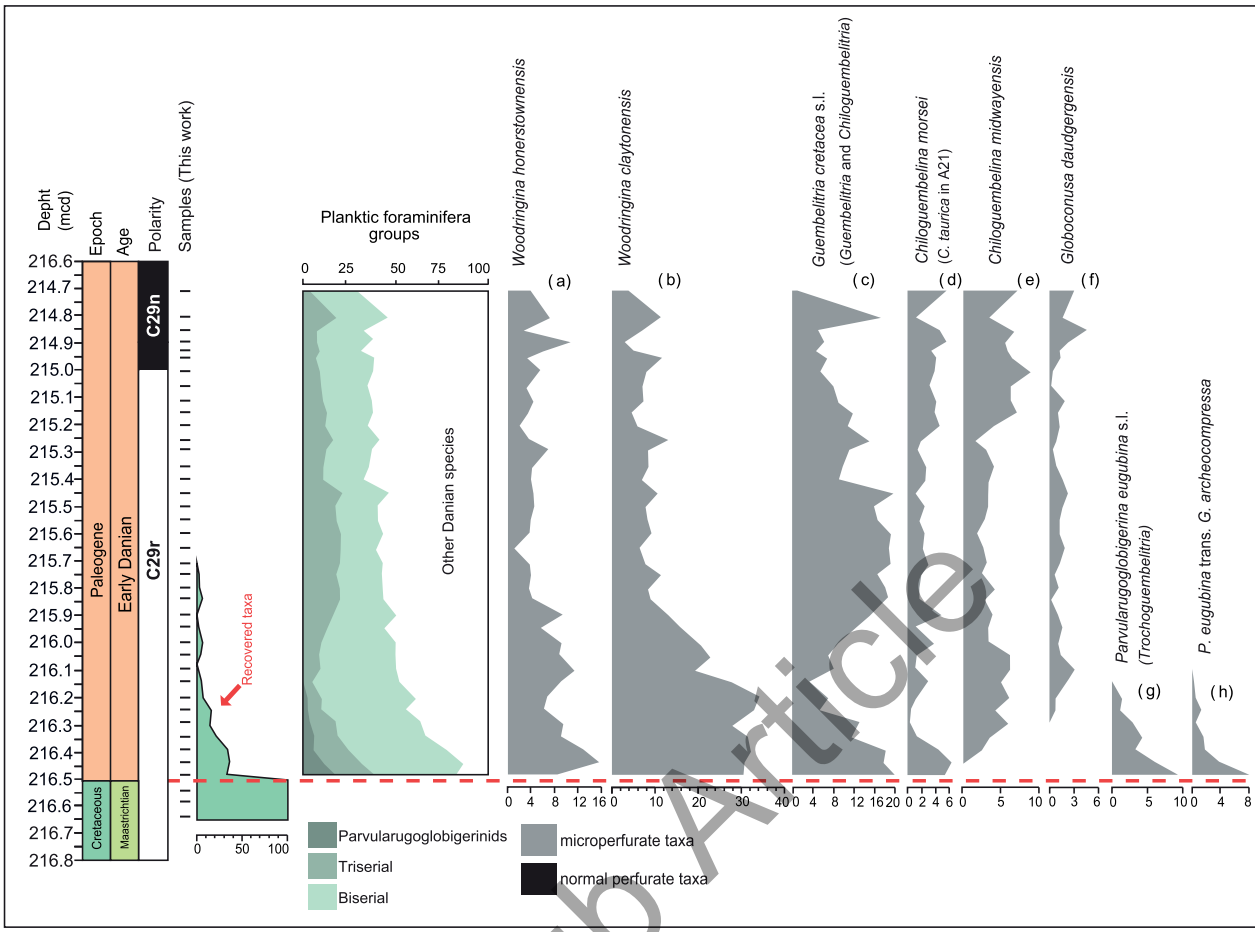

Fig. 5. Relative abundances (%) at Site 1262B of the Danian planktic foraminiferal species and groups: parvularugoglobigerinids s. l. (*Parvularugoglobigerina* s. s. and *Trochoguembelitria*), biserial (*Woodringina* and *Chiloguembelina*), triserial (*Guembelitria* s. s. and *Chiloguembelitria*) and other genera (*Globoconusa*, *Eoglobigerina*, *Subbotina*, *Parasubbotina*, *Praemurica*, and *Globanomalina*). All relative abundances of planktic foraminifera are arranged from 5a to 5r. Danian planktic foraminiferal zones of W11 (Wade et al. 2011) and A21 (Arenillas et al. 2021). P. har. = *Pseudoguembelina hariaensis* Zone *sensu* Nederbragt (1991).

hyperthermal events (e. g., Leon-Rodriguez and Dickens 2010, Luciani et al. 2010, Coccioni et al. 2012, Coccioni et al. 2019, Galazzo et al. 2013, D'Onofrio et al. 2016, Deprez et al. 2017, Intxauspe-Zubiaurre et al. 2018). At Site 1262, the P/B ratio dropped, and the FI values increased moderately during the Dan-C2 event (Fig. 2), suggesting a change in the carbonate saturation state that could be related to a transient increase in ocean acidification, similar to what was observed at DSDP Site 516F (Rio Grande Rise, South Atlantic; Krahl et al. 2020). According to Kucera et al. (1997), the FI values associated with strong carbonate dissolution for the Maastrichtian of the Walvis Ridge and Rio Grande Rise are usually > 40 %. This result was obtained by using more lenient criteria for calculating FI than this study, considering only those specimens that preserve less than half of their test as fragments. Nevertheless, based on stricter criteria (see above), we observe that the FI values at Site 1262 oscillate around 16 % during Dan-C2 (Fig. 2, Appendix B), similar to the low FI values reported for the Dan-C2 interval at Caravaca (Gilabert et al. 2021). We observed dissolution features in planktic foraminiferal tests, such as abrasion marks, broken and/or isolated chambers, and corroded walls (Fig. 6, sample C), although they were not abundant. We thus suggest that carbonate dissolution was low to moderate within the Danian interval at Site 1262. Our interpretation is compatible with those based on Fe enrichments (Barnet et al. 2019) and well-preserved calcareous benthic foraminiferal assem-

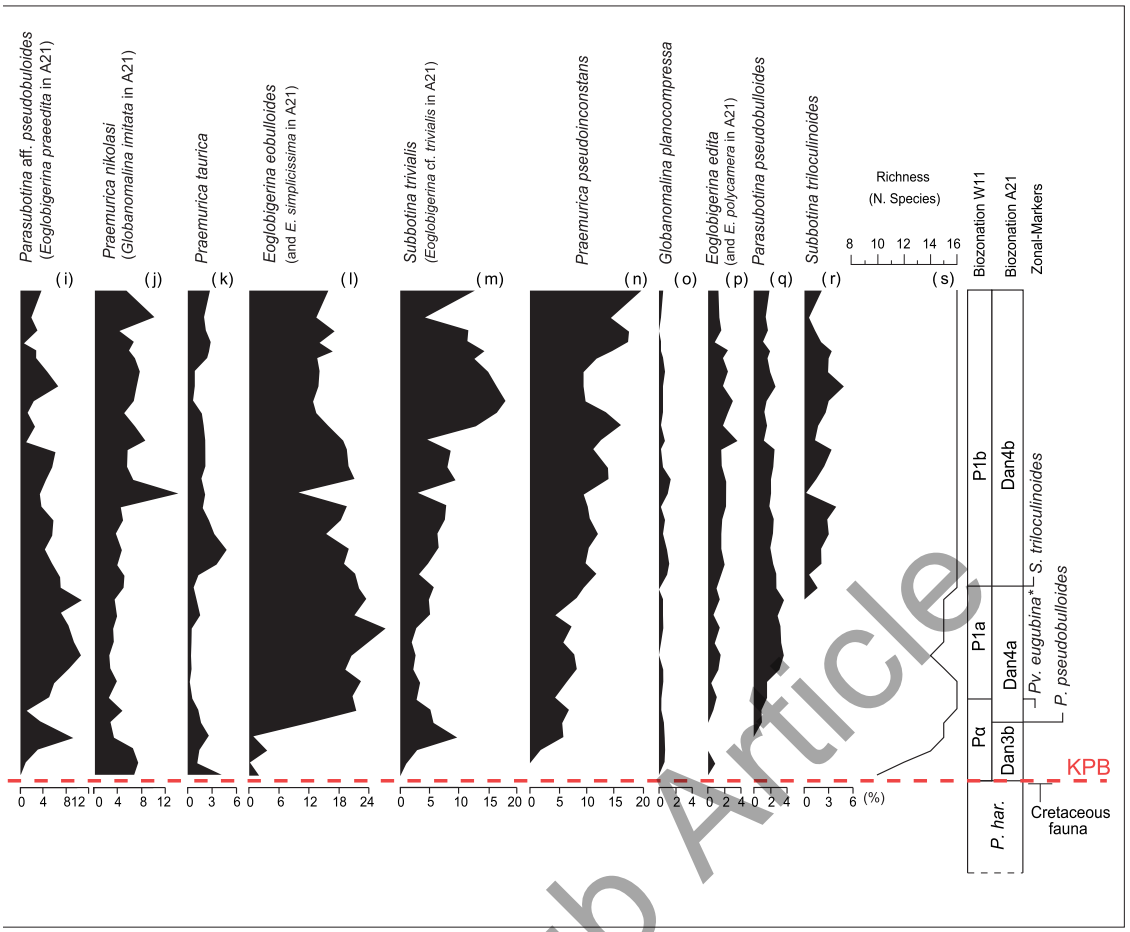

blages, which were not significantly affected by the Dan-C2 event (Arreguín-Rodríguez et al. 2021), suggesting deposition above the CCD.

Mercury concentrations and TOC values at Site 1262 show weak negative correlation (r = –0.194; Fig. 9a). The fact that there is no covariation between Hg and TOC suggests that TOC enrichments are not solely responsible for Hg accumulation in the section, supporting a volcanic Hg source. TOC values <0.2 %, such as those at Site 1262 (Fig. 2, Appendix D), can also generate artificial Hg/TOC peaks (Grasby et al. 2019). However, we consider this possibility unlikely due to the strong resemblance between the records of the Hg concentration and the Hg/TOC ratio (Fig. 2). In fact, the Hg concentration can be controlled by redox conditions (Shen et al. 2019). We used the Mn concentrations as a proxy for redox conditions (e. g., Yao et al. 2021). These exhibit a low positive correlation (r = 0.464; Fig. 9c) with Hg concentrations at Site 1262, suggesting that seafloor oxygenation had no significant influence on Hg enrichments.

The Hg concentration in sediments can be also affected by diagenesis. We used $\delta^{18}O_{bulk}$ values as indicators of diagenetic intensity, since these can be significantly altered by changes in carbonate precipitation (Watkins et al. 2014) or during extensive carbonate diagenesis (Swart 2015). At Site 1262B, no significant covariation was observed for Hg content and $\delta^{18}O_{bulk}$ (r = 0.435; Fig. 9b), suggesting that none of these diagenetic processes was responsible for the

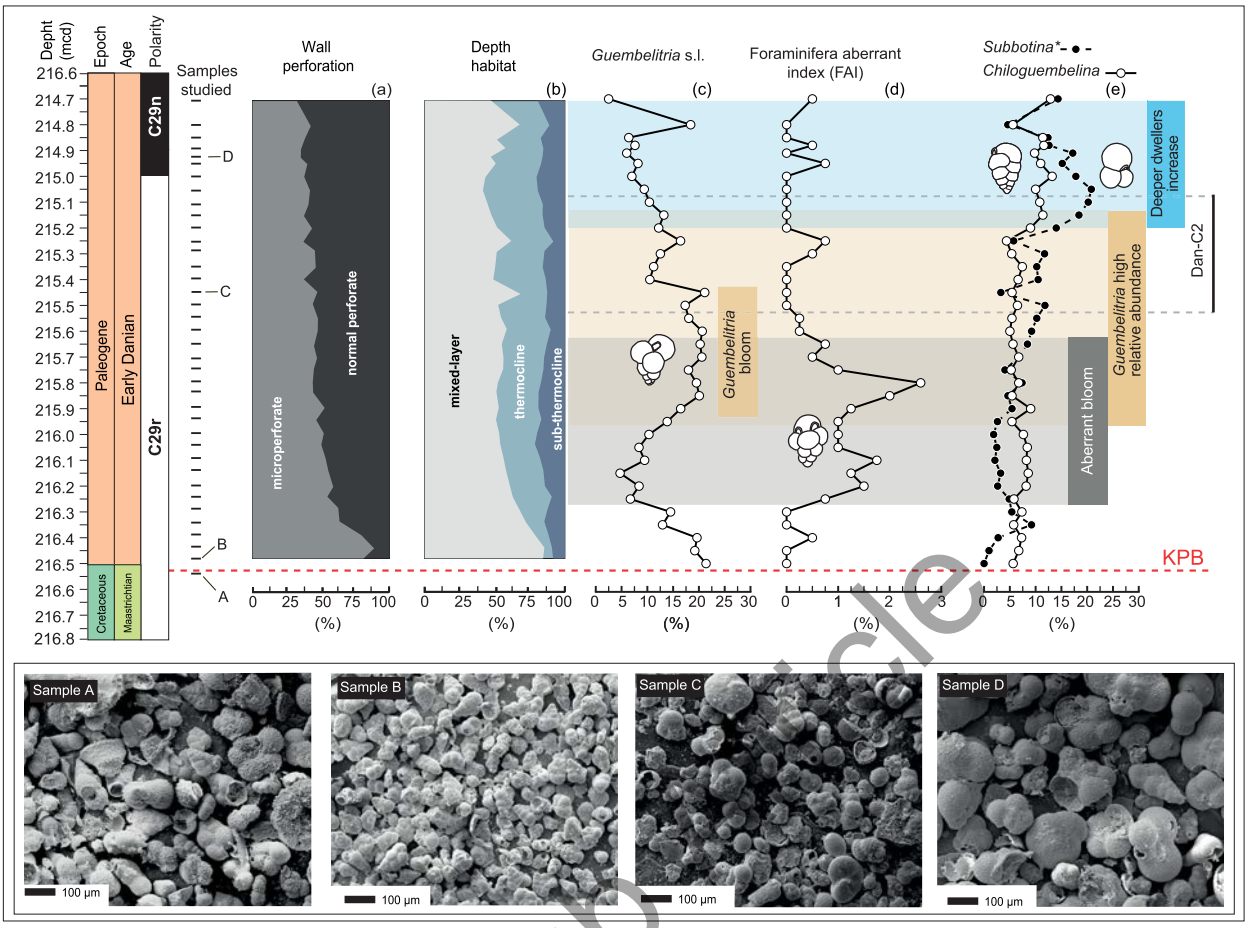

Fig. 6. Main changes in the planktic foraminiferal assemblages occurring at Site 1262 during the early Danian. a) Relative abundance (%) of planktic foraminiferal taxa according to their wall perforation (microperforate *vs.* macroperforate); b) Abundance of planktic foraminiferal taxa according to their depth habitat, which is related to the stratification of the upper water column; c) Relative abundance (%) in triserial guembelitriids (*Guembelitria* s. s. and *Chiloguembelitria*); d) Foraminiferal abnormality index (FAI): relative abundance (%) in aberrant planktic foraminiferal specimens; e) Relative abundances (%) in *Subbotina* and *Chiloguembelina*; *Subbotina**: species *trivialis* has been included in *Subbotina* according to the W11 taxonomy, but the A21 taxonomy assigned it to the genus *Eoglobigerina* (*E.* cf. *trivialis*). Scanning electron microscope (SEM) detail of samples A to D (identified in the time axis) showing the overall trend of planktic foraminiferal test sizes and the main biogenic components in the studied interval at Site 1262. Sample A = large-sized planktic foraminiferal assemblage of the Maastrichtian; Sample B = reduced sizes of planktic foraminifera just after the K/Pg boundary; Sample C = biogenic constituents with presence of calcispheres within the Dan-C2 interval; Sample D = increased sizes of planktic foraminiferal tests after the Dan-C2 event.

Hg enrichments. We thus suggest that the Hg accumulation in the early Danian sediments at Site 1262 was mainly controlled by the global intensity of volcanic emissions.

4.3. Stepwise recovery of early Danian planktic foraminiferal assemblages

The lowermost planktic foraminiferal assemblages identified at Site 1262, recorded within the first 25 cm above the K/Pg boundary (upper part of Biozone Pα, or Subbiozone Dan3b), were dominated by microperforated genera such as *Woodringina* (Fig. 5a–b), *Guembelitria* s. l. (Fig. 5c), and *Parvularugoglobigerina* s. l. (Fig. 5g–h), which inhabited the mixed-layer in the surface ocean (D'Hondt and Zachos 1993, Olsson et al. 1999, Lowery et al. 2021). These assemblages suggest that eutrophic conditions occurred in the upper water column during this time interval, in accordance with observations from the Chicxulub

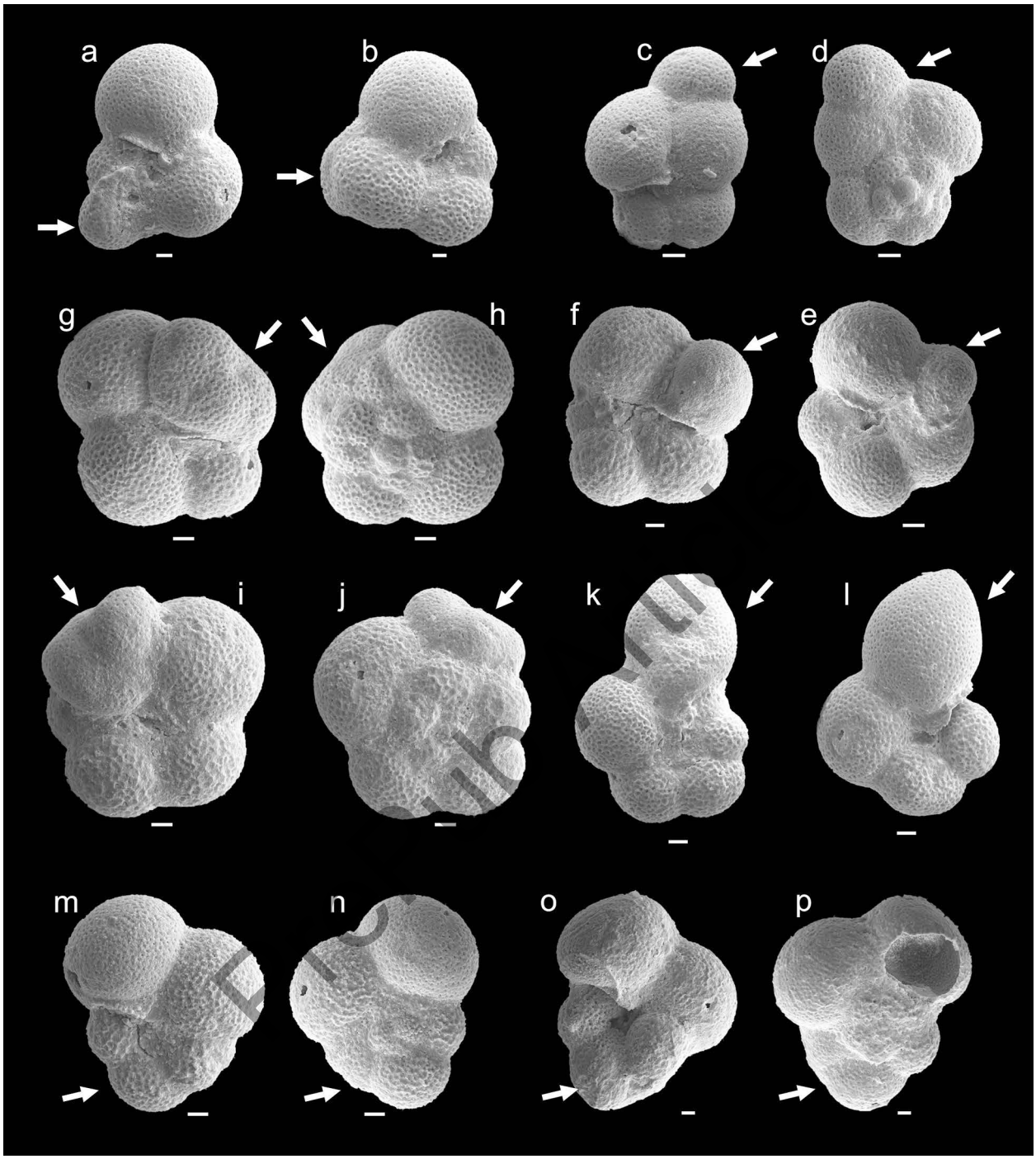

Fig. 7. SEM micrographs of planktic foraminifera with test abnormalities from Site 1262 (scale bars = 10 μm). a. *Subbotina* spp. (215.68 mcd). b. *Subbotina* spp. (216.03 mcd). c–d. *Parasubbotina* spp. (215.93 mcd). e. *Parasubbotina* or *Eoglobigerina* spp. (216.58 mcd). f. *Eoglobigerina* spp. (215.98 mcd). g–h. *Parasubbotina* spp. (216.03 mcd). i–j. *Parasubbotina pseudobulloides* (215.13 mcd). k. *Parasubbotina* spp. (215.93 mcd). l. *Praemurica* spp. (216.03 mcd). m–n. *Eoglobigerina* spp. (215.68 mcd). o–p. *Praemurica pseudoinconstans* (216.03 mcd). Arrows indicate morphological abnormalities.

impact site (Jones et al. 2019; Lowery et al. 2021). The dominance of mixed-layer planktic foraminiferal taxa after the K/Pg boundary was a consequence of global collapse of the marine biological pump and its subsequent restoration (Birch et al. 2016). In the earliest Danian, less export productivity and thus enhanced

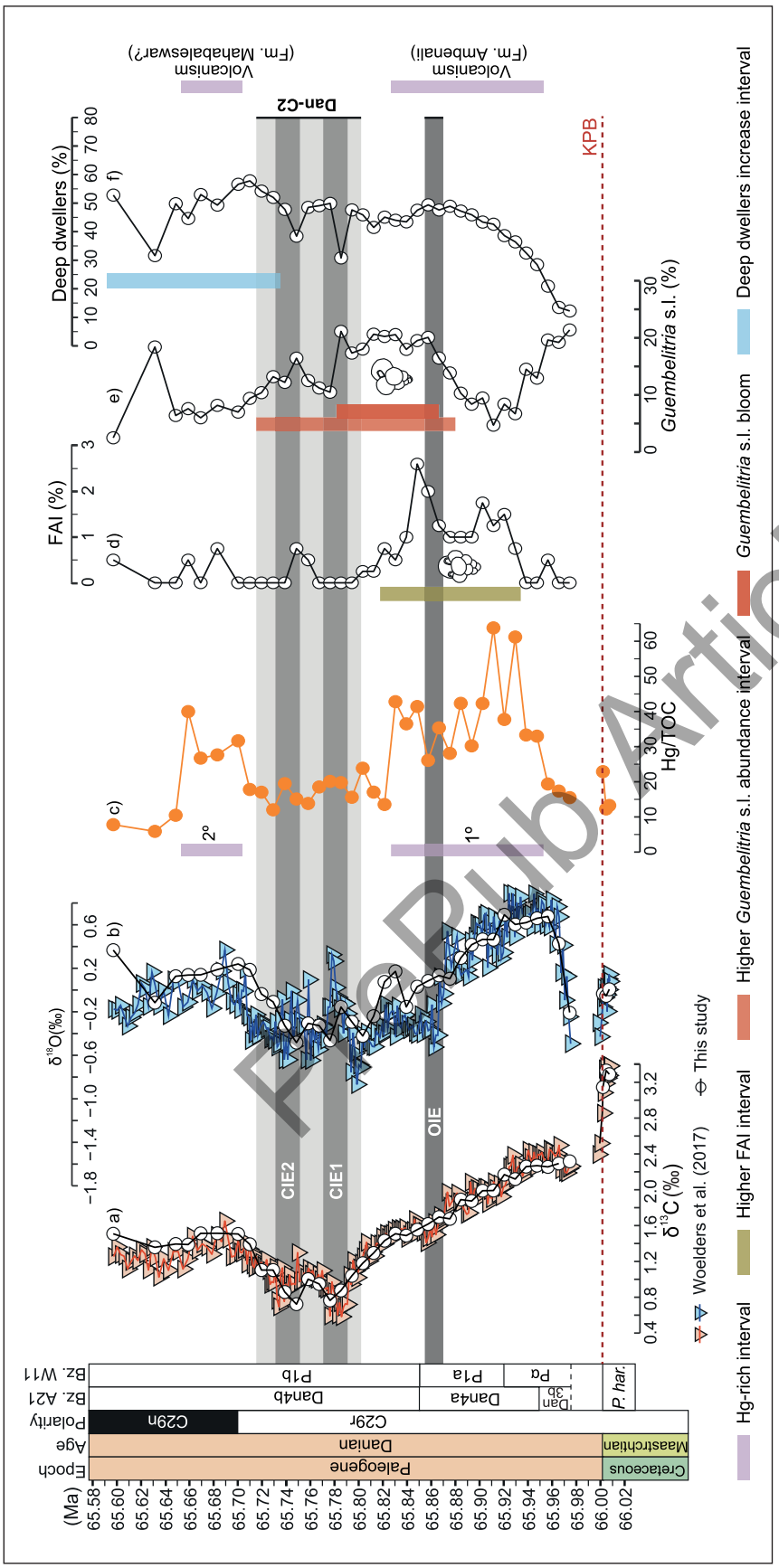

Fig. 8. Main changes in planktic foraminiferal assemblages and geochemical proxies during the early Danian at Site 1262, according to the age model here proposed. a–b. bulk sediment carbon and oxygen stable isotopes from this work and Woelders et al. (2017); c. Hg/TOC ratio; d. Foraminiferal abnormality index (FAI); e. Relative abundances (%) in *Guembelitria* s. l. [*Chiloguembelitria*]; f. Relative abundances (%) in deep-dwelling taxa (thermocline + sub-thermocline dwellers; see Appendix C for further details).

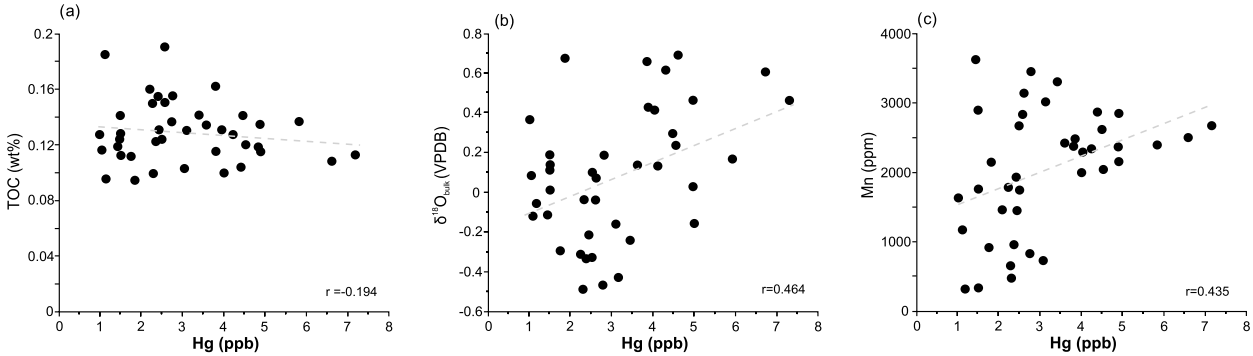

Fig. 9. Crossplots of Hg concentrations versus TOC (a), $\delta^{18}O_{bulk}$ (b), and Mn concentrations (c). Pearson correlations (r) are also shown.

remineralization of organic matter in the surface ocean would have favored the proliferation of mixed-layer taxa (Jones et al. 2019).

After this first interval, no significant variations in species richness were observed at Site 1262, implying that the Dan-C2 event and the DT volcanism had a low impact on planktic foraminiferal species richness (Fig. 5). A rapid increase in the abundance of deep-dwelling taxa (thermocline dwellers as *Eoglobigerina*, *Chiloguembelina*, *Globanomalina* and sub-thermocline dwellers as *Parasubbotina pseudobulloides*; Aze et al. 2011, Appendix C), occurred ~65.93 Ma (216.25 mcd), i. e., ~70 kyr after the K/Pg boundary (Fig. 8f). This suggests increased stratification in the water column from that time on, which was not significantly interrupted by the Dan-C2 event or by the DT volcanic activity. The relative abundance of *Subbotina* and *Chiloguembelina* increased ~272 kyr after the K/Pg boundary (~65.729 Ma, 215.15 mcd), rising from 5.97 to 15.35 % in *Subbotina* and from 6.62 to 10.77 % in *Chiloguembelina* (Fig. 6). Within the deep-dwellers (Fig. 8f), *Chiloguembelina* and *Subbotina* (Berggren and Norris 1997, Coxall et al. 2000, Luciani et al. 2020) increased their relative abundance, suggesting a recovery of the pelagic ecosystem towards the end of the Dan-C2 event with increased stratification of the water column (Gilabert et al. 2021, Lowery et al. 2021). According to Birch et al. (2016, 2021), the first phase of partial recovery of the $\delta^{13}C$ gradient between the surface and deep ocean occurred about ~270 kyr after the K/Pg boundary (~215.15 mcd in Site 1262). This recovery phase is almost coeval with the increases in abundance of *Subbotina* and *Chiloguembelina*, as well as with an increase in the overall test sizes of planktic foraminifera at Site 1262 (Fig. 6, sample D).

4.4. Links between the Dan-C2 event and Deccan Traps (DT) volcanic activity?

The mercury chemostratigraphy at Site 1262 allows us to identify two intervals during the early Danian with high Hg concentrations that can be linked to the increased DT volcanic activity. The first Hg-rich interval is dated to between 65.952 (216.375 mcd) and 65.825 Ma (215.675 mcd), i. e., between 49 and 176 kyr after the K/Pg boundary (Fig. 8c, Appendix D). Both the onset and the end of this Hg-rich interval preceded the onset of the Dan-C2 event (65.798 Ma) by about 154 and 27 kyr respectively. These observations suggest that the stressing paleoenvironmental conditions in the upper water column linked to DT volcanism ended shortly before the onset of the Dan-C2 event. In fact, considering the ages and the uncertainty of the radiometric dating (±64 kyr, U-Pb; ±213 kyr, $^{40}Ar/^{39}Ar$) calculated by Schoene et al. (2021), the first Hg-rich interval at Site 1262 correlates well with the emplacement of the Ambenali Fm. (~65.95 Ma, Fig. 8). Since this Hg-rich interval does not coincide with the Dan-C2 interval at Site 1262, we can conclude that there was no direct temporal link between the Dan-C2 event and the emplacement of the Ambenali Fm., as Gilabert et al. (2022) already proposed.

The second Hg-rich interval began almost at the C29r/C29n boundary (215 mcd, 65.700 Ma) (Figs 2 and 8), and specifically occurred between 65.705 Ma (215.02 mcd) and 65.653 Ma (214.86 mcd), i. e., between 296 and 348 kyr after the K/Pg boundary (Fig. 8c, Appendix D). This second Hg-rich interval is notably shorter (52 kyr) than the first one (127 kyr), and its average Hg/TOC value is appreciably lower (31.5) than that of the first one (43). Although it could also be genetically related to higher volcanic activity in

the DT, this second Hg-rich interval had a very weak influence on the climate, since no relevant isotopic event is associated with it (Fig. 8). Moreover, it did not influence the ocean environments either, since no relevant turnovers in the planktic foraminifera assemblages are observed (Fig. 5). The DT volcanic episode closest to the second Hg-rich interval is the one that produced the Mahabaleshwar Fm., whose emplacement began ~65.62 Ma (Schoene et al. 2019, Sprain et al. 2019), i. e., 381 kyr after the K/Pg boundary. The estimated difference of ~30 kyr between the end of the second Hg-rich interval and the onset of the emplacement of the Mahabaleshwar Fm. prevents us from establishing a robust link between the two episodes. Nevertheless, if the hole studied (Hole 1262B) had a small hiatus affecting the lowermost part of the magnetozone C29n, the second Hg-rich interval would consequently be more modern and could be coeval to emplacement of the Mahabaleshwar Fm. Another possible explanation could be terminal reactivation of the Ambenali eruptive episode. The reactivation of a DT volcanic formation is more difficult to explain according to the mega-pulse eruptive model of Schoene et al. (2019). Instead, this feature could be more consistent with the quasi-continuous eruption model of Sprain et al. (2019).

4.5. Environmental disruptions linked to the volcanic activity

Recent studies have explored a possible relationship between increased abundances of aberrant planktic foraminiferal specimens (increased FAI) with a proliferation of triserial guembelitriids in the early Danian and intervals of higher volcanic activity, which can tentatively be related to enrichment in toxic heavy metals such as Hg (e. g., Arenillas et al. 2018, Gilabert et al. 2021). Our multiproxy approach at Site 1262 lends further support to the idea that DT volcanic emissions, recorded as Hg-rich intervals, are one of the main environmental stress factors that potentially caused disturbances in the planktic foraminiferal assemblages during the early Danian.

In accordance with the readjusted age model for Site 1262 proposed here, increased relative abundances of aberrant planktic foraminiferal specimens occurred at Site 1262 between ~65.934 (216.27 mcd) and ~65.817 Ma (215.62 mcd), i. e., between ~67 and ~184 kyr after the K/Pg boundary (Fig. 8d), coinciding approximately with the first Hg-rich interval identified. At Site 1262, species with a higher abundance in aberrant tests belong to thermocline and subthermocline dwellers including *Eoglobigerina*, *Parasubbotina*, and *Subbotina* (Fig. 7), which is unlike other localities at or near continental margins, such as Caravaca and Zumaia (Spain) or El Kef (Tunisia), where the aberrant specimens are more common among mixed-layer dweller *Guembelitria* s. l. and FAI values are much more anomalous, around 10 times larger (Arenillas et al. 2018, Gilabert et al. 2021). Several environmental stressors can potentially cause morphological abnormalities in planktic foraminiferal tests, including increases in temperature, eutrophy and/or acidity of ocean waters (Mancin and Darling 2015, Arenillas et al. 2018). Among recent foraminifera, contamination by heavy metals and trace elements is considered one of the most likely causes for such abnormalities (e. g., Coccioni et al. 2009, Frontalini et al. 2009). Since no relevant changes in temperature, acidity, and nutrient supply are observed across this interval (Figs 6 and 8), we suggest that the main cause of this increase in aberrant specimens was contamination by heavy metals from the DT volcanic emissions. The inefficient biological pump during this interval could contribute to extend over time, on a ~10^4 years scale, the recycling and remineralization of heavy metals and other trace elements at the ocean surface, in a mechanism similar to that proposed by Jiang et al. (2010) to explain why ejecta metals remained dissolved in the surface ocean for thousands or tens of thousands of years after the Chicxulub impact at the K/Pg boundary.

We have also identified a bloom of triserial guembelitriids (Fig. 8e), preceding the Dan-C2 event, between ~65.872 (215.92 mcd) and ~65.781 Ma (215.42 mcd), i. e., between ~129 and 220 kyr after the K/Pg boundary (Figs 6c and 8e). Similar blooms of triserial guembelitriids have been reported before the Dan-C2 event at Contessa Highway (Coccioni et al. 2010), DSDP Site 577 (Pacific Ocean; Smit and Romein 1985), Agost (Spain; Canudo et al. 1991), Caravaca and Zumaia (Gilabert et al. 2021, Gilabert et al. 2022), ODP Site 528 (South Atlantic Ocean; D'Hondt and Keller 1991), and El Kef (Arenillas et al. 2018). Triserial guembelitriids are considered opportunists that inhabited surface waters and thrived under high-stress environmental conditions, proliferating on continental margins and near volcanic areas where nutrients are abundant, whether they are of upwelling, continental or volcanic origin (Kroon and Nederbragt 1990, Pardo and Keller 2008, Keller and Pardo 2004). Consequently, a remarkable envir-

onmental change at the ocean surface of the South Atlantic Ocean is required to explain the proliferation of guembelitriids in an oceanic pelagic environment away from continental margins as Site 1262 (Fig. 8). However, at Site 1262, the triserial guembelitriid bloom started (~62 kyr) and ended (~36 kyr) later than the increased FAI interval (Fig. 8d), unlike what is recorded in pelagic sections placed at or near the continental margins (e. g. Caravaca, Zumaia and El Kef) where both intervals coincide (Arenillas et al. 2018, Gilabert et al. 2021, Gilabert et al. 2022). The cause-effect relationship between the DT volcanism, marked by the Hg-rich and increased FAI interval, and the guembelitriid proliferation is therefore difficult to establish at Site 1262, so a different mechanism or a different environmental stressor is required.

Remarkable changes in benthic foraminiferal assemblages at Site 1262 were reported before the Dan-C2 interval (Arreguín-Rodríguez et al. 2021), approximately coinciding with the triserial guembelitriid bloom. The authors reported that the predominant benthic foraminiferal taxa during this interval were indicative of environmental instability and an enhanced food supply to seafloor. Similarly, Bralower et al. (2020) also identified changes in the calcareous nannoplankton assemblages, such as the proliferation of the calcareous dinocyst *Cervisella*, which, as *Guembelitria* s. l., is an opportunistic taxon that preferably inhabited continental margins with high nutrient availability. At Site 1262, the triserial guembelitriid bloom coincides with a high abundance of thermocline and sub-thermocline planktic foraminiferal taxa, such as *Eoglobigerina*, *Parasubbotina*, and *Subbotina* (Fig. 6b), and of the nannofossil *Braarudosphaera* (Bralower et al. 2020), indicating that the bloom occurred during a time interval with a well-stratified water column. Consequently, the environmental change that caused the proliferation of guembelitriids at Site 1262 seems to have affected only the ocean surface.

Bralower et al. (2020) reported deposition of microcrystalline calcite structures, at Site 1262 and at many other localities, evidencing a second global acme of microbial phytoplankton (probably cyanobacteria) after the one that occurred immediately after the K/Pg boundary event. At Site 1262, this second microbial bloom is recorded between ~65.93 (216.28 mcd) and ~65.90 Ma (216.08 mcd), i. e., between 71 and 101 kyr after the K/Pg boundary. Kulal et al. (2020), among others, reported that the microbial activity can remove toxic heavy metals from water. We propose consequently that the bloom of microbial activity helped remove Hg and other toxics from the surface ocean, explaining why the malformations primarily affected thermocline and sub-thermocline dwellers at Site 1262. In addition, the maximum in microbial activity occurred towards the end of the first Hg-rich interval and the beginning of the bloom of opportunist planktic taxa, such as *Cervisella* and *Guembelitria* s. l. This microbial maximum could not only help remove toxic elements but also increase the nutrient availability in the surface ocean, favoring the proliferation of nannoplankton and planktic foraminiferal opportunistic taxa (Bralower et at. 2020; this study).

The nutrient availability in the surface ocean could also be higher due to the inefficient biological pump (Henehan et al. 2019). The very low transfer efficiency (quantity of organic matter that sinks below 1000 m; Henson et al. 2012, Lowery et al. 2021) allowed the recycling and remineralization of the nutrients to continue at the ocean surface. The low transfer efficiency at Site 1262 would explain why the $\Delta^{13}C$ gradient in the water column is locally low, and why the benthic foraminiferal assemblages indicate low food supply to the sea floor before microbial and triserial guembelitriid blooms (Arreguín-Rodríguez et al. 2021).

We suggest, therefore that the emplacement of Ambenali Fm. could be the cause of the increase in Hg and aberrant specimens, whereas the triserial guembelitriid bloom seems to be more closely linked to an increase in microbial activity that provided additional food supply to the ocean surface. If the extra nutrient source that triggered the increased microbial activity was also from the DT volcanism, the weak biological pump during all this interval could be the reason that, in oceanic pelagic environments such as that of Site 1262, there was a lag between the increased FAI interval and the triserial guembelitriid bloom. Unlike what occurs in localities placed at or near the continental margins, the inefficient biological pump at Site 1262 could lead to sustained recycling and remineralization of organic matter in the surface ocean, causing the microbial bloom to occur ~20 kyr later than the beginning of increased DT volcanic activity. The microbial activity increased only when the volcanic nutrient supply was a little higher, and the triserial guembelitriid bloom lasted for 36 kyr after the end of this DT eruptive phase, because the biological pump, although improved, was still inefficient, allowing nutrients to be recycled and to remain in the surface ocean.

Another environmental factor that could have favored the triserial guembelitriid bloom was the increase in ocean surface temperatures at ~65.87 Ma (215.92 mcd), i. e., 131 kyr after the K/Pg boundary and 72 kyr before the beginning of Dan-C2 event, as suggested by the $\delta^{18}O$ record at Site 1262 (Fig. 2 and Fig. 8b; and Appendix A). In the early Danian, the changes in the ocean surface temperature seem to have been mainly linked to orbital forcing, especially modulated by 405-kyr and 100-kyr eccentricity (Gilabert et al. 2022, and references herein). At Site 1262 (Fig. 8), the earliest part of triserial guembelitriid bloom (between ~131 and 176 kyr after the K/Pg boundary) seems to coincide with an interval in which the DT volcanic activity is still high and the ocean surface temperature increased. Subsequently, the relative abundance in triserial guembelitriids decreased (Fig. 8e), but remained high until almost the end of the Dan-C2 interval, suggesting that the main environmental stressor in the surface ocean was temperature.

Based on the earliest Danian planktic foraminiferal assemblages from Site 1262, we suggest that unstable conditions in the water column prior to the Dan-C2 event were probably associated with the emplacement of the Ambenali Fm., as Gilabert et al. (2021, 2022) have previously proposed. As mentioned above, the onset of the emplacement of the Ambenali Fm. occurred at ~65.95 Ma (Schoene et al. 2019, Sprain et al. 2019), approximately 50 kyr after the K/Pg boundary, and it lasted for the next ~100 kyr according to Schoene et al. (2019, 2021) or ~330 kyr according to Sprain et al. (2019). Our results show a better correspondence with the mega-pulse model of Schoene et al. (2019) than with the quasi-continuous model of Sprain et al. (2019), since the proxies of increased volcanic activity (Hg and Hg/TOC anomalies) and the greater environmental stress (increased FAI and triserial guembelitriid bloom) seem to be coeval with a shorter emplacement time of the Ambenali Fm. (Figs 6 and 8). Except maybe for the increased microbial activity and triserial guembelitriid bloom, the paleobiological response to the emplacement of the Ambelani Fm. was apparently quite weak (Figs 6 and 8). It was a response similar to those reported for the Maastrichtian DT volcanic phases, such as the one associated to the emplacement of the Kalsubai subgroup between ~66.30 and 66.10 Ma (Schoene et al. 2019, Sprain et al. 2019) that was one of the triggers of the Late Maastrichtian Warming Event (Barnet et al. 2018, Gilabert et al. 2021b, Gilabert et al. 2022).

5. Conclusions

Detailed analyses of the planktic foraminiferal assemblages, including the foraminiferal abnormality index (FAI), the fragmentation index (FI), and the P/B ratio, and of several geochemical proxies, including $\delta^{13}C$, $\delta^{18}O$, $CaCO_3$%, Mn, Hg, and the Hg/TOC ratio, were carried out at Site 1262 (South Atlantic) for the first ~400 kyr of the early Danian. This multiproxy study allowed us to recognize the most relevant changes in climate, ocean surface environment, and water column structure at Site 1262 during this interval. On the basis of the $\delta^{13}C$ and $\delta^{18}O$ data (reported here and in previous works), the paleoclimatic Dan-C2 event is recognized between ~65.80 and ~65.71 Ma.

Two intervals with Hg and Hg/TOC anomalies are identified at Site 1262 and interpreted as evidence of higher volcanic activity linked to the Deccan Traps (DT). The first Hg-rich interval, which was the longer and greater Hg anomaly, occurred between ~65.95 and 65.82 Ma, preceding the onset of the Dan-C2 event by ~40 kyr. The second Hg-rich interval, which was shorter and smaller, occurred between ~65.70 and 65.65 Ma, beginning near the end of Dan-C2 and ending notably later. In light of the age model here reported for Site 1262 and the latest radiometric dating of the DT volcanic formations, we can conclude that there was no direct temporal link between the Dan-C2 event and the massive DT volcanism, whereas the first Hg-rich interval seems strongly linked to the emplacement of the Ambenali Formation of the Deccan Traps. The origin of the second Hg-rich interval is still unclear, but could be related to the emplacement of the Mahabaleshwar Fm.

Higher values in aberrant planktic foraminiferal abundance (FAI) are documented only during the first Hg-rich interval, suggesting an increased contamination by heavy metal poisoning from the DT volcanic emissions, specifically during the emplacement of the Ambenali Fm. In addition, a triserial guembelitriid bloom occurred between ~65.87 and ~65.78 Ma, also preceding the Dan-C2 event but lagging with respect to the interval of high Hg content and increased FAI. The lag at Site 1262 between both intervals can be explain by a combination of several environmental factors, such as the inefficient biological pump, the increase in temperatures, and the increase in the microbial activity and food supply to the ocean surface, the latter perhaps still linked to the terminal volcanic emissions linked to the Ambelani Fm. During the Dan-C2 event, environmental stress seems to have been considerably reduced,

although the continuing high abundance of triserial guembelitriids denotes environmental instability, perhaps related to higher ocean surface temperatures. From the Dan-C2 event to the end of the interval studied, no evidence of environmental stress is recognized. Conversely, we observed a progressive increase in the relative abundance of species that inhabited the thermocline from the middle part of Dan-C2, suggesting a progressive stratification and stabilization of the water column. All these evidences suggest that, although volcanism may have had an impact on planktic foraminiferal assemblages in the early Danian through metal contamination, marine ecosystems likely became progressively more stable and resistant to changes in volcanic emissions and the carbon cycle.

Acknowledgements. We thank the editor, Joerg Pross, and the three reviewers, Chris Lowery, Andy Fraass and an anonymous reviewer, for thoughtful and constructive reviews which improved the manuscript. We deeply thank Sietske Batenburg for support. Felipe Toledo and Maria A. Pivel is thanked for early review and sugestions. We are grateful to the International Ocean Discovery Program (IODP) for providing the studied samples, and to Capes for providing the postgraduate grant for G. Krahl and M. H. H. Bom. This research is part of the grants PGC2018-093890-B-I00 and PID2022-136233NB-I00 funded by MCIN/AEI/10.13039/501100011033 and by ERDF A way of making Europe, and DGA group E33_20R funded by the Aragonese Government and by ERDF A way of making Europe. Vicente Gilabert acknowledges support from Ministerio de Universidades (MIU) and European Union (Margarita Salas post-doctoral grant) funded by European Union-NextGeneration EU. We thank R. Glasgow for improving the English text.

References

Alegret, L., Thomas, E., & Lohmann, K. C. (2012). End-Cretaceous marine mass extinction not caused by productivity collapse. *Proceedings of the National Academy of Sciences of the United States of America*, *109*(3), 728–732. https://doi.org/10.1073/pnas.1110601109

Alvarez, L. W., Alvarez, W., Asaro, F., & Michel, H. V. (1980). Extraterrestrial cause for the Cretaceous-Tertiary extinction. *Science*, *208*(4448), 1095–1108. https://doi.org/10.1126/science.208.4448.1095

Arenillas, I., & Arz, J. A. (2017). Benthic origin and earliest evolution of the first planktonic foraminifera after the Cretaceous/Paleogene boundary mass extinction. *Historical Biology*, *29*(1), 17–24. https://doi.org/10.1080/08912963.2015.1119133

Arenillas, I., Arz, J. A., & Gilabert, V. (2018). Blooms of aberrant planktic foraminifera across the K/Pg boundary in the Western Tethys: Causes and evolutionary implications. *Paleobiology*, *44*(3), 1–17. https://doi.org/10.1017/pab.2018.16

Arenillas, I., Arz, J. A., Metsana-Oussaid, F., Gilabert, V., & Belhai, D. (2022). Hypothesis testing on the planktic foraminiferal survival model after the KPB extinction: Evidence from Tunisia and Algeria. *Fossil Record (Weinheim)*, *25*(1), 43–63. https://doi.org/10.3897/fr.25.79958

Arenillas, I., Arz, J. A., Molina, E., & Dupuis, C. (2000a). The Cretaceous/Paleogene (K/P) boundary at Aïn Settara, Tunisia: Sudden catastrophic mass extinction in planktic foraminifera. *Journal of Foraminiferal Research*, *30*(3), 202–218. https://doi.org/10.2113/0300202

Arenillas, I., Arz, J. A., Molina, E., & Dupuis, C. (2000b). An independent test of planktic foraminiferal turnover across the Cretaceous/Paleogene (K/P) boundary at El Kef, Tunisia: Catastrophic mass extinction and possible survivorship. *Micropaleontology*, *46*(1), 31–49.

Arenillas, I., Gilabert, V., & Arz, J. A. (2021). New biochronological scales of planktic foraminifera for the early Danian based on high-resolution biostratigraphy. *Geosciences*, *11*(11), 1–26. https://doi.org/10.3390/geosciences11110479

Arreguín-Rodríguez, G. J., Barnet, J. S. K., Leng, M. J., Littler, K., Kroon, D., Schmidt, D. N., … Alegret, L. (2021). Benthic foraminiferal turnover across the Dan-C2 event in the eastern South Atlantic Ocean (ODP Site 1262). *Palaeogeography, Palaeoclimatology, Palaeoecology*, *572*, 1–15. https://doi.org/10.1016/j.palaeo.2021.110410

Arz, J. A., Arenillas, I., Grajales-Nishimura, J. M., Liesa, C. L., Soria, A. R., Rojas, R., … Gilabert, V. (2022 in press). No evidence of multiple impact scenario across the Cretaceous/Paleogene boundary based on planktic foraminiferal biochronology. In C. Koeberl, P. Claeys, & S. Montanari (Eds.) *From the Guajira desert to the Apennines, and from Mediterranean microplates to the Mexican killer asteroid: Honoring the Career of Walter Alvarez, GSA Special paper 557*, https://doi.org/10.1130/2022.2557(20)

Aze, T., Ezard, T. H. G., Purvis, A., Coxall, H. K., Stewart, R. M., Wade, B. S., & Pearson, P. N. (2011). A phylogeny of Cenozoic macroperforate planktonic foraminifera from fossil data. *Biological Reviews of the Cambridge Philosophical Society*, *86*(4), 900–927. https://doi.org/10.1111/j.1469-185X.2011.00178.x

Barnet, J. S. K., Littler, K., Kroon, D., Leng, M. J., Westerhold, T., Rohl, U., & Zachos, J. C. (2017). A new high-resolution chronology for the late Maastrichtian warming event: Establishing robust temporal links with the onset of Deccan volcanism. *Geology*, *46*(2), 147–150. https://doi.org/10.1130/G39771.1

Barnet, J. S. K., Littler, K., Westerhold, T., Kroon, D., Leng, M. J., Bailey, I., … Zachos, J. C. (2019). A high-fidelity benthic stable isotope record of late Cretaceous early Eocene climate change and carbon-cycling. *Paleoceanography and Paleoclimatology*, *34*(4), 672–691. https://doi.org/10.1029/2019PA003556

Batenburg, S. J., Friedrich, O., Moriya, K., Voigt, S., Cournède, C., Blum, P., … Wilson, P. A., (2018). Late Maastrichtian carbon isotope stratigraphy and cyclostratigraphy of the Newfoundland Margin (Site U1403, IODP Leg 342). *Newsletters on Stratigraphy*, *51*(2), 245e260. https://doi.org/10.1127/nos/2017/0398.

Berger, W. H., & Diester-Haass, L. (1988). Paleoproductivity: The benthic/planktonic ratio in foraminifera as a productivity index. *Marine Geology*, *81*(1-4), 15–25. https://doi.org/10.1016/0025-3227(88)90014-X

Berggren, W. A., & Norris, R. D. (1997). Biostratigraphy, phylogeny and systematics of Paleocene trochospiral planktic foraminifera. *Micropaleontology*, *43*, 1–116. https://doi.org/10.2307/1485988

Berggren, W. A., & Pearson, P. N. (2005). A revised tropical and subtropical Paleogene planktonic foraminiferal zonation. *Journal of Foraminiferal Research*, *35*(4), 279–298. https://doi.org/10.2113/35.4.279

Birch, H., Schmidt, D. N., Coxall, H. K., Kroon, D., & Ridgwell, A. (2021). Ecosystem function after the K/Pg extinction: decoupling of marine carbon pump and diversity. *Proceeding of The Royal Society Bulletin*, *288*, 20210863. https://doi.org/10.1098/rspb.2021.0863

Birch, H. S., Coxall, H. K., Pearson, P. N., Kroon, D., & Schmidt, D. N. (2016). Partial collapse of the marine carbon pump after the Cretaceous-Paleogene boundary. *Geology*, *44*(4), 287–290. https://doi.org/10.1130/G37581.1

Boersma, A., & Silva, I. P. (1983). Paleocene planktonic foraminiferal biogeography and the paleooceanography of the Atlantic Ocean. *Micropaleontology*, *29*(4), 355–381. https://doi.org/10.2307/1485514

Bornemann, A., Jehle, S., Lägel, F., Deprez, A., Petrizzo, M. R., & Speijer, R. P. (2021). Planktic foraminiferal response to an early Paleocene transient warming event and biostratigraphic implications. *International Journal of Earth Sciences*, *110*(2), 583–594. https://doi.org/10.1007/s00531-020-01972-z

Bowles, J. (2006). Data report: revised magnetostratigraphy and magnetic mineralogy of sediments from Walvis Ridge, Leg 208. In D. Kroon, J. C. Zachos, & C. Richter (Eds.), Proc. ODP, Sci. Results: *Vol. 208*. *Ocean Drilling Program* (pp. 1–24). College Station, TX. https://doi.org/10.2973/odp.proc.sr.208.206.2006

Bralower, T. J., Cosmidis, J., Heaney, P. J., Kump, L. R., Morgan, J. V., Harper, D. T., … Vajda, V. (2020). Origin of a global carbonate layer deposited in the aftermath of the Cretaceous-Paleogene boundary impact. *Earth and Planetary Science Letters*, *548*, 116476. https://doi.org/10.1016/j.epsl.2020.116476

Canudo, J. I., Keller, G., & Molina, E. (1991). Cretaceous/Tertiary boundary extinction pattern and faunal turnover at Agost and Caravaca, S. E. Spain. *Marine Micropaleontology*, *17*(3-4), 319–341. https://doi.org/10.1016/0377-8398(91)90019-3

Coccioni, R., Bancalà, G., Catanzarit, R., Fornaciari, E., Frontalini, F., Giusberti, L., … Sprovieri, M. (2012). An integrated stratigraphic record of the Palaeocene–lower Eocene at Gubbio (Italy): New insights into the early Palaeogene hyperthermals and carbon isotope excursions. *Terra Nova*, *24*(5), 380–386. https://doi.org/10.1111/j.1365-3121.2012.01076.x

Coccioni, R., Frontalini, F., Bancalà, G., Fornaciari, E., Jovane, L., & Sprovieri, M. (2010). The Dan-C2 hyperthermal event at Gubbio (Italy): Global implications, environmental effects, and cause(s). *Earth and Planetary Science Letters*, *297*(1-2), 298–305. https://doi.org/10.1016/j.epsl.2010.06.031

Coccioni, R., Frontalini, F., Catanzariti, R., Jovane, L., Rodelli, D., Rodrigues, I. M. M., … Galbrun, B. (2019). Paleoenvironmental signature of the Selandian-Thanetian Transition Event (STTE) and Early Late Paleocene Event (ELPE) in the Contessa Road section (western Neo-Tethys). *Palaeogeography, Palaeoclimatology, Palaeoecology*, *523*(1), 62–77. https://doi.org/10.1016/j.palaeo.2019.03.023

Coccioni, R., Frontalini, F., Marsili, A., & Mana, D. (2009). Benthic foraminifera and trace element distribution: A case-study from the heavily polluted lagoon of Venice (Italy). *Marine Pollution Bulletin*, *59*(8-12), 257–267. https://doi.org/10.1016/j.marpolbul.2009.08.009

Coxall, H., D'Hondt, S., & Zachos, J. (2006). Pelagic evolution and environmental recovery after the Cretaceous-Paleogene mass extinction. *Geology*, *34*(4), 297–300. https://doi.org/10.1130/G21702.1

Coxall, H., Pearson, P. N., Shackleton, N. J., & Hall, M. (2000). Hantkeninid depth adaptation; an evolving life strategy in a changing ocean. *Geology*, *28*(1), 87–90. https://doi.org/10.1130/0091-7613(2000)28<87:HDAAELL>2.0.CO;2

Deprez, A., Jehle, S., Bornemann, A., & Speijer, R. P. (2017). Pronounced biotic and environmental change across the latest Danian warming event (LDE) at Shatsky Rise, Pacific Ocean (ODP Site 1210). *Marine Micropaleontology*, *137*, 31–45. https://doi.org/10.1016/j.marmicro.2017.10.001

Dinarès-Turell, J., Westerhold, T., Pujalte, V., Röhl, U., & Kroon, D. (2014). Astronomical calibration of the Danian stage (early Paleocene) revisited: Settling chronologies of sedimentary records across the Atlantic and Pacific Oceans. *Earth and Planetary Science Letters*, *405*, 119–131. https://doi.org/10.1016/j.epsl.2014.08.027

D'Hondt, J. (2005). Consequences of the Cretaceous/Paleogene Mass Extinction for Marine Ecosystems. *Annual Review of Ecology, Evolution, and Systematics*, *36*(1), 295–317. https://doi.org/10.1146/annurev.ecolsys.35.021103.105715

D'Hondt, S., & Keller, G. (1991). Some patterns of planktic foraminiferal assemblage turnover at the Cretaceous-Tertiary boundary. *Marine Micropaleontology*, *17*(1-2), 77–118. https://doi.org/10.1016/0377-8398(91)90024-Z

D'Hondt, S., & Zachos, J. C. (1993). On Stable Isotopic Variation and Earliest Paleocene Planktonic Foraminifera. *Paleoceanography*, *8*(4), 527–547. https://doi.org/10.1029/93PA00952

D'Onofrio, R., Luciani, V., Fornaciari, E., Giusberti, L., Galazzo, F. B., Dallanave, E., … Telch, S. (2016). En-

vironmental perturbation at the early Eocene ETM2, H2, and I1 events as inferred by Tethian calcareous plankton (Terche section, northeastern Italy). *Paleoceanography*, *31*(9), 1225–1247. https://doi.org/10.1002/2016PA002940

Font, E., Adatte, T., Sial, A. N., Lacerda, L. D., Keller, G., & Punekar, J. (2016). Mercury anomaly, Deccan Volcanism and the end-Cretaceous Mass Extinction. *Geology*, *44*(2), 171–174. https://doi.org/10.1130/G37451.1

Frontalini, F., Buosi, C., Da Pelo, S., Coccioni, R., Cherchi, A., & Bucci, C. (2009). Benthic foraminifera as bio-indicators of trace element pollution in the heavily contaminated Santa Gilla lagoon (Cagliari, Italy). *Marine Pollution Bulletin*, *58*(6), 858–877. https://doi.org/10.1016/j.marpolbul.2009.01.015

Galazzo, F. B., Giusberti, L., Luciani, V., & Thomas, E. (2013). Paleoenvironmental changes during the Middle Eocene Climatic Optimum (MECO) and its aftermath: The benthic foraminiferal record from the Alano section (NE Italy). *Palaeogeography, Palaeoclimatology, Palaeoecology*, *378*, 22–35. https://doi.org/10.1016/j.palaeo.2013.03.018

Gilabert, V., Arenillas, I., Arz, J. A., Batenburg, S. J., & Robinson, S. A. (2021a). Multiproxy analysis of paleoenvironmental, paleoclimatic and paleoceanographic changes during the early Danian in the Caravaca section (Spain). *Palaeogeography, Palaeoclimatology, Palaeoecology*, *576*, 110513. https://doi.org/10.1016/j.palaeo.2021.110513

Gilabert, V., Arz, J. A., Arenillas, I., Robinson, S. A., & Ferrer, D. (2021b). Influence of the Latest Maastrichtian Warming Event on planktic foraminiferal assemblages and ocean carbonate saturation at Caravaca, Spain. *Cretaceous Research*, *125*, 104844. https://doi.org/10.1016/j.cretres.2021.104844

Gilabert, V., Batenburg, S. J., Arenillas, I., & Arz, J. A. (2022). Contribution of orbital forcing and Deccan volcanism to global climatic and biotic changes across the Cretaceous-Paleogene boundary at Zumaia, Spain. *Geology*, *50*(1), 21–25. https://doi.org/10.1130/G49214.1

Gradstein, F., Ogg, J., Schmitz, M., & Ogg, G. (2020). *Geological time Scale 2020*. Elsevier.

Grasby, S. E., Them, T. R., II,, Chen, Z., Yin, R., & Ardakani, O. H. (2019). Mercury as a proxy for volcanic emissions in the geologic record. *Earth-Science Reviews*, *196*, 102880. https://doi.org/10.1016/j.earscirev.2019.102880

Hancock, H. J. L., & Dickens, G. R. (2005). Carbonate dissolution episodes in Paleocene and Eocene sediment, Shatsky Rise, west-central Pacific. In T. J. Bralower, I. Premoli Silva, & M. J. Malone (Eds.), *Proceedings of the Ocean Drilling Program, Scientific Results 198.*. Texas A & M Univ., College Station, pp. 1–24. Available at World Wide Web. odp.tamu.edu/publications/198_SR/116/116.htm

Hildebrand, A. R., Penfield, G. T., Kring, D. A., Pilkington, M., Camargo Z., A., Jacobson, S. B., & Boynton, W. V. (1991). Chicxulub crater: A possible Cretaceous/Tertiary boundary impact crater on the Yucatan peninsula, Mexico. *Geology*, *19*(9), 867–871. https://doi.org/10.1130/0091-7613(1991)0192.3.CO;2

Huber, B. T., & Boersma, A. (1994). Cretaceous origination of *Zeauvigerina* and its relationship to Paleocene Biserial planktonic foraminifera. *Journal of Foraminiferal Research*, *41*(4), 268–287. https://doi.org/10.2113/gsjfr.24.4.268

Huber, B. T., & Quillévéré, F. (2005). Revised Paleogene planktonic foraminiferal biozonation for the Austral Realm. *Journal of Foraminiferal Research*, *35*(4), 299–314. https://doi.org/10.2113/35.4.299

Huber, B., Petrizzo, M. R., & MacLeod, K. (2020). Planktonic Foraminiferal Endemism at Southern High Latitudes Following the Terminal Cretaceous Extinction. *Journal of Foraminiferal Research*, *50*(4), 382–402. https://doi.org/10.2113/gsjfr.50.4.382

Hull, P. M., Bornemann, A., Penman, D. E., Henehan, M. J., Norris, R. D., Wilson, P. A., … Zachos, J. C. (2020). On impact and volcanism across the Cretaceous-Paleogene boundary. *Science*, *367*(6475), 266–272. https://doi.org/10.1126/science.aay5055

Henson, S. A., Sanders, R., & Madsen, E. (2012). Global patterns in efficiency of particulate organic carbon export and transfer to the deep ocean. *Global Biogeochemical Cycles*, *26*(1), GB1028. https://doi.org/10.1029/2011GB004099

Intxauspe-Zubiaurre, B., Martinez-Braceras, N., Payros, A., Ortiz, S., Dinarès-Turell, J., & Flores, J. A. (2018). The last Eocene hyperthermal (Chron C19r event, ~41.5 Ma): Chronological and paleoenvironmental insights from a continental margin (Cape Oyambre, N Spain). *Palaeogeography, Palaeoclimatology, Palaeoecology*, *505*, 198–216. https://doi.org/10.1016/j.palaeo.2018.05.044

Jehle, S., Bornemann, A., Deprez, A., & Speijer, R. P. (2015). The Impact of the Lasted Danian Event on Planktic Foraminiferal Faunas at ODP Site 1210 (Shatsky Rise, Pacific Ocean). *PLoS One*, *10*(11), e0141644. https://doi.org/10.1371/journal.pone.0141644

Jehle, S., Bornemann, A., Lägel, A. F., Deprez, A., & Speijer, R. P. (2019). Paleoceanographic changes across the Latest Danian Event in the South Atlantic Ocean and planktic foraminiferal response. *Palaeogeography, Palaeoclimatology, Palaeoecology*, *525*, 1–13. https://doi.org/10.1016/j.palaeo.2019.03.024

Jones, H. L., Lowery, C. M., & Bralower, T. J. (2019). Delayed calcareous nannoplankton boom-bust successions in the earliest Paleocene Chicxulub (Mexico). *Geology*, *47*(8), 753–756. https://doi.org/10.1130/G46143.1

Keller, G., & Pardo, A. (2004). Age and paleoenvironmental of the Cenomanian-Turonian global stratotype section and point at Pueblo, Colorado. *Marine Micropaleontology*, *51*(1-2), 95–128. https://doi.org/10.1016/j.marmicro.2003.08.004

Keller, G., Mateo, P., Monkenbusch, J., Thibault, N., Punekar, J., Spangenberg, J. E., … Adatte, T. (2020). Mercury linked to Deccan Traps volcanism, climate change and the end-Cretaceous mass extinction. *Global and*

Planetary Change, *194*, 103312. https://doi.org/10.1016/j.gloplacha.2020.103312

Keller, G., Mateo, P., Punekar, J., Khozyem, H., Gertsch, B., Spangenberg, J., … Adatte, T. (2018). Environmental changes during the Cretaceous-Paleogene mass extinction and Paleocene-Eocene Thermal Maximum: Implications for the Anthropocene. *Gondwana Research*, *56*, 69–89. https://doi.org/10.1016/j.gr.2017.12.002

Koutsoukos, E. A. M. (1996). The Cretaceous-Tertiary boundary at Poty, NE Brazil-event stratigraphy and palaeoenvironments. *Centres de Recherches Exploration-Production Elf-Aquitaine, Bulletin*, *16*, 413–431.

Koutsoukos, E. A. M. (2014). Phenotypic plasticity, speciation, and phylogeny in early Danian planktic foraminifera. *Journal of Foraminiferal Research*, *44*(2), 109–142. https://doi.org/10.2113/gsjfr.44.2.109

Krahl, G., Bom, M. H. H., Kochhann, K. G. D., Souza, L. V., Savian, J. F., & Fauth, G. (2020). Environmental changes occurred during the early Danian at the Rio Grande Rise, South Atlantic Ocean. *Global and Planetary Change*, *191*, 103197. https://doi.org/10.1016/j.gloplacha.2020.103197

Kring, D. A. (2007). The Chicxulub impact event and its environmental consequences at the Cretaceous/Tertiary boundary. *Palaeogeography, Palaeoclimatology, Palaeoecology*, *255*(1-2), 4–21. https://doi.org/10.1016/j.palaeo.2007.02.037

Kroon, D., & Nederbragt, A. J. (1990). Ecology and paleoecology of triserial planktic foraminifera. *Marine Micropaleontology*, *16*(1-2), 25–38. https://doi.org/10.1016/0377-8398(90)90027-J

Kroon, D., & Zachos, J. C. et al. (2007). 1. Leg 208 synthesis: Cenozoic climate cycles and excursions. In D. Kroon, J. C. Zachos, & C. Richter (Eds.), *Proceedings of the Ocean Drilling Program, Scientific Results*, *208*, pp. 1–55.

Kucera, M., Malmgren, B. A., & Sturesson, U. (1997). Foraminiferal dissolution at shallow depths of the Walvis Ridge and Rio Grande Rise during the latest Cretaceous: Inferences for deep-water circulation in the South Atlantic. *Palaeogeography, Palaeoclimatology, Palaeoecology*, *129*(3-4), 195–212. https://doi.org/10.1016/S0031-0182(96)00133-2

Kulal, D. K., Loni, P. C., Dcosta, C., Some, S., & Kalambate, P. K. (2020). Cyanobacteria: as a promising candidate for heavy-metals removal. *Advances in Cyanobacterial Biology*, 291–300. https://doi.org/10.1016/B978-0-12-819311-2.00019-X

Laskar, J., Gastineau, M., Delisle, J.-B., Farrés, A., & Fienga, A. (2011). Strong chaos induced by close encounters with Ceres and Vesta. *Astronomy & Astrophysics*, *532*, L4. https://doi.org/10.1051/0004-6361/201117504

Leighton, A. D., Hart, M. B., Smart, C. W., Leng, M. J., & Hampton, M. (2017). Timing Recovery after the Cretaceous/Paleogene Boundary: Evidence from the Brazos River, Texas, USA. *Journal of Foraminiferal Research*, *47*(3), 229–238. https://doi.org/10.2113/gsjfr.47.3.229

Leon-Rodriguez, L., & Dickens, G. R. (2010). Constraints on ocean acidification associated with rapid and massive carbon injections: The early Paleogene record at ocean drilling program site 1215, equatorial Pacific Ocean. *Palaeogeography, Palaeoclimatology, Palaeoecology*, *298*(3-4), 409–420. https://doi.org/10.1016/j.palaeo.2010.10.029

Lowery, C. M., & Fraass, J. S. (2019). Morphospace expansion paces taxonomic diversification after end Cretaceous mass extinction. *Nature Ecology & Evolution*, *3*(6), 900–904. https://doi.org/10.1038/s41559-019-0835-0

Lowery, C. M., Bralower, T. J., Owens, J. D., Rodríguez-Tovar, F. J., Jones, H., Smit, J., … Zylberman, W. (2018). Rapid recovery of life at ground zero of the end-Cretaceous mass extinction. *Nature*, *558*(7709), 288–291. https://doi.org/10.1038/s41586-018-0163-6

Lowery, C. M., Jones, H. L., Bralower, T., Cruz, L. P., Gebhardt, C., Whalen, M. T., … Gulick, S. P. S. (2021). Early Paleocene Paleoceanography and Export Productivity in the Chicxulub Crater. *Paleoceanography, Paleoclimatology*, *36*(11).

Luciani, V., D'Onofrio, R., Dickens, G. R., & Wade, B. S. (2017). Planktic foraminiferal response to early Eocene carbon cycle perturbations in the southeast Atlantic Ocean (ODP Site 1263). *Global and Planetary Change*, *158*, 119–133. https://doi.org/10.1016/j.gloplacha.2017.09.007

Luciani, V., D'Onofrio, R., Filippi, G., & Moretti, S. (2020). Which was the habitat of early Eocene planktic foraminifer *Chiloguembelina*? Stable isotope paleobiology from th Atlantic Ocean and implication for paleoceanographic reconstructions. *Global and Planetary Change*, *191*, 103216. https://doi.org/10.1016/j.gloplacha.2020.103216

Luciani, V., Giusberti, L., Agnini, C., Fornaciari, E., Rio, D., Spofforth, D. J. A., & Pälike, H. (2010). Ecological and evolutionary response of Tethyan planktonic foraminifera to the middle Eocene climatic optimum (MECO) from the Alano section (NE Italy). *Palaeogeography, Palaeoclimatology, Palaeoecology*, *292*(1-2), 82–95. https://doi.org/10.1016/j.palaeo.2010.03.029

Mancin, N., & Darling, K. (2015). Morphological abnormalities of planktonic foraminiferal tests in the SW Pacific Ocean over the last 550ky. *Marine Micropaleontology*, *120*, 1–19. https://doi.org/10.1016/j.marmicro.2015.08.003

Molina, E. (2015). Evidence and causes of the main extinction events in the Paleogene based on extinction and survival patterns of foraminifera. *Earth-Science Reviews*, *140*, 166–181. https://doi.org/10.1016/j.earscirev.2014.11.008

Molina, E., Alegret, L., Arenillas, I., Arz, J. A., Gallala, N., Grajales-Nishimura, M., … Zaghbib-Turki, D. (2009). The Global Boundary Stratotype Section and Point for the base of the Danian Stage (Paleocene, Paleogene, "Tertiary", Cenozoic): Auxiliary sections and correlation. *Episodes*, *32*(2), 84–95. https://doi.org/10.18814/epiiugs/2009/v32i2/002

Molina, E., Arenillas, I., & Arz, J. A. (1996). The Cretaceous/Tertiary boundary mass extinction in planktic foraminifera at Agost (Spain). *Revue de Micropaleontologie*, *39*(3), 225–243. https://doi.org/10.1016/S0035-1598(96)90075-6

Morgan, J. V., Bralower, T. J., Brugger, J., & Wünnemann, K. (2022). The Chicxulub impact and its environmental consequences. *Nature Reviews. Earth & Environment*, *3*(5), 338–354. https://doi.org/10.1038/s43017-022-00283-y

Nederbragt, A. J. (1991). Late Cretaceous biostratigraphy and development of Heterohelicidae (planktic foraminifera). *Micropaleontology*, *37*(4), 329–372. https://doi.org/10.2307/1485910

Nguyen, T. M. P., & Speijer, R. P. (2014). A new procedure to assess dissolution based on experiments on Pliocene–Quaternary foraminifera (ODP Leg 160, Eratosthenes Seamount, Eastern Mediterranean). *Marine Micropaleontology*, *106*, 22–39. https://doi.org/10.1016/j.marmicro.2013.11.004

Norris, R. D., Huber, B. T., & Self-Trail, J. (1999). Synchroneity of the K-T oceanic mass extinction and meteorite impact: Blake Nose, western North. *Geology*, *27*(5), 419–422. https://doi.org/10.1130/0091-7613(1999)027<0419:SOTKTO>2.3.CO;2

Olsson, R. K., Berggren, W. A., Hemleben, C., & Huber, B. T. (1999). Atlas of Paleocene Planktonic Foraminifera. *Smithsonian Contributions to Paleobiology*, 1–252./ https://doi.org/10.5479/si.00810266.85.1

Orth, C. J., Gilmore, J. S., Knight, J. D., Pillmore, C. L., Tschudy, R. H., & Fassett, J. E. (1981). An iridium abundance anomaly at the palynological Cretaceous-Tertiary boundary in northern New Mexico. *Science*, *214*(4527), 1341–1343. https://doi.org/10.1126/science.214.4527.1341

Pardo, A., & Keller, G. (2008). Biotic effects of environmental catastrophes at the end of the Cretaceous and early Tertiary: *Guembelitria* and *Heterohelix* blooms. *Cretaceous Research*, *29*(5-6), 1058–1073. https://doi.org/10.1016/j.cretres.2008.05.031

Punekar, J., Mateo, P., & Keller, G. (2014). Effects of Deccan volcanism on paleoenvironment and planktic foraminifera: A global survey. *Geological Society of America. Special Paper*, (505). https://doi.org/10.1130/2014.2505(04)

Quillévéré, F., Norris, R. D., Kroon, D., & Wilson, P. A. (2008). Transient ocean warming and shifts in carbon reservoirs during the early Danian. *Earth and Planetary Science Letters*, *265*(3-4), 600–615. https://doi.org/10.1016/j.epsl.2007.10.040

Ravizza, G., & Peucker-Ehrenbrink, B. (2003). Chemostratigraphic evidence of Deccan volcanism from the marine Os isotope record. *Science*, *302*(5649), 1392–1395. https://doi.org/10.1126/science.1089209

Ravizza, G., & Vonderhaar, D. (2012). A geochemical clock in earliest Paleogene pelagic carbonates based on the impact induced Os isotope excursion at the Cretaceous-Paleogene boundary. *Paleoceanography*, *27*(3), PA3219. https://doi.org/10.1029/2012PA002301

Robinson, N., Ravizza, G., Coccioni, R., Peucker-Ehrenbrink, B., & Norris, R. (2009). A high-resolution marine 187Os/188Os record for the late Maastrichtian: Distinguishing the chemical fingerprints of the Deccan and KT impact event. *Earth and Planetary Science Letters*, *281*, 159–168. https://doi.org/10.1016/j.epsl.2009.02.019

Schoene, B., Eddy, M. P., Keller, C. B., & Samperton, K. M. (2021). An evaluation of deccan traps eruption rates using geochronologic data. *Geochronology*, *3*(1), 181–198. https://doi.org/10.5194/gchron-3-181-2021

Schoene, B., Eddy, M. P., Samperton, K. M., Keller, C. B., Keller, G., Adatte, T., & Khadri, S. F. R. (2019). U-Pb constraints on pulsed eruption of the Deccan Traps across the end-Cretaceous mass extinction. *Science*, *363*(6429), 862–866. https://doi.org/10.1126/science.aau2422

Schulte, P., Alegret, L., Arenillas, I., Arz, J. A., Barton, P. J., Bown, P. R., … Willumsen, P. S. (2010). The Chicxulub asteroid impact and mass extinction at the Cretaceous-Paleogene boundary. *Science*, *327*(5970), 1214–1218. https://doi.org/10.1126/science.1177265

Sheehan, P. M., Coorough, P. J., & Fastovsky, D. E. (1996). Biotic selectivityduring the K/T and Late Ordovician extinction events. In G. Ryder, D. Fastovsky, & S. Gartner (Eds.), Geological Society of America Special Papers: *Vol. 307. The Cretaceous-Tertiary Event and Other Catastrophes in Earth History* (pp. 477–489).

Shen, J., Algeo, T. J., Planavsky, N. J., Yu, J., Feng, Q., Song, H., … Chen, J. (2019). Mercury enrichments provide evidence of Early Triassic volcanism following the End-Permian mass extinction. *Earth-Science Reviews*, *195*, 191–212. https://doi.org/10.1016/j.earscirev.2019.05.010

Sial, A. N., Chen, J., Lacerda, L. D., Frei, R., Tewari, V. C., Pandit, M. K., … Pereira, N. S. (2016). Mercury enrichment and Hg isotopes in Cretaceous–Paleogene boundary successions: Links to volcanism and palaeoenvironmental impacts. *Cretaceous Research*, *66*, 60–81. https://doi.org/10.1016/j.cretres.2016.05.006

Sial, A. N., Lacerda, L. D., Ferreira, V. P., Frei, R., Marquillas, R. A., Barbosa, J. A., … Pereira, N. S. (2013). Mercury as a proxy for volcanic activity during extreme environmental turnover: The Cretaceous–Paleogene transition. *Palaeogeography, Palaeoclimatology, Palaeoecology*, *387*, 153–164. https://doi.org/10.1016/j.palaeo.2013.07.019

Smit, J. (1982). Geological Society of America Special Papers: *Vol. 190*. *Extinction and evolution of planktonic foraminifera after a major impact at the Cretaceous/Tertiary boundary* (pp. 329–352), https://doi.org/10.1130/SPE190-p329

Smit, J., & Romein, A. J. T. (1985). A sequence of events across the Cretaceous-Tertiary boundary. *Earth and Planetary Science Letters*, *74*(2-3), 155–170. https://doi.org/10.1016/0012-821X(85)90019-6

Sprain, C. J., Renne, P. R., Vanderkluysen, L., Pande, K., Self, S., & Mittal, T. (2019). The eruptive tempo of Deccan volcanism in relation to the Cretaceous-Paleogene boundary. *Science*, *363*(6429), 866–870. https://doi.org/10.1126/science.aav1446

Swart, P. K. (2015). The geochemistry of carbonate diagenesis: The past, present and future. *Sedimentology*, *62*(5), 1233–1304. https://doi.org/10.1111/sed.12205

Stax, R., & Stein, R. (1993). Long-term changes in the accumulation of organic carbon in Neogene sediments, Ontong Java Plateau. *Proceedings of the Ocean Drilling Program*, *130*, 573–579. https://doi.org/10.2973/odp.proc.sr.130.039.1993

Thibault, N., Galbrun, B., Gardin, S., Minoletti, F., & Le Callonnec, L. L. (2016). The end- Cretaceous in the southwestern Tethys (Elles, Tunisia): Orbital calibration of paleoenvironmental events before the mass extinction. *International Journal of Earth Sciences*, *105*(3), 771–795. https://doi.org/10.1007/s00531-015-1192-0

Van der Zwaan, G. J., Jorissen, F. J., & De Stigter, H. C. (1990). The depth dependency of planktonic/benthic foraminiferal ratios: Constraints and applications. *Marine Geology*, *95*(1), 1–16. https://doi.org/10.1016/0025-3227(90)90016-D

Van Hinsbergen, D. J. J., Groot, L. V., Van Schaik, J. S., Spakman, W., Bijl, P. K., Sluijs, A., … Brinkhuis, H. (2015). A Paleolatitude Calculator for Paleoclimate Studies. *PLoS One*, *10*(6), e0126946. https://doi.org/10.1371/journal.pone.0126946

Wade, B. S., Pearson, P. N., Berggren, W. A., & Pälike, H. (2011). Review and revision of Cenozoic tropical planktonic foraminiferal biostratigraphy and calibration to the geomagnetic polarity and astronomical time scale. *Earth-Science Reviews*, *104*(1-3), 111–142. https://doi.org/10.1016/j.earscirev.2010.09.003

Watkins, J. M., Hunt, J. D., Ryerson, F. J., & DePaolo, D. J. (2014). The influence of temperature, pH, and growth rate on the $\delta^{18}O$ composition of inorganically precipitated calcite. *Earth and Planetary Science Letters*, *404*, 332–343. https://doi.org/10.1016/j.epsl.2014.07.036

Westerhold, T., Marwan, N., Drury, A. J., Liebrand, D., Agnini, C., Anagnostou, E., … Zachos, J. C. (2020). An astronomically dated record of Earth's climate and its predictability over the last 66 million years. *Science*, *369*(6509), 1383–1387. https://doi.org/10.1126/science.aba6853

Westerhold, T., Röhl, U., Donner, B., McCarren, H. K., & Zachos, J. C. (2011). A complete high-resolution Paleocene benthic stable isotope record for the Central Pacific (ODP site 1209). *Paleoceanography*, *26*(2), PA2216. https://doi.org/10.1029/2010PA002092

Westerhold, T., Röhl, U., Raffi, I., Fornaciari, E., Monechi, S., Reale, V., … Evans, H. F. (2008). Astronomical calibration of the Paleocene time. *Palaeogeography, Palaeoclimatology, Palaeoecology*, *257*(4), 377–403. https://doi.org/10.1016/j.palaeo.2007.09.016

Woelders, L., Vellekoop, J., Kroon, D., Smit, J., Casadío, S., Prámparo, M., … Speijer, R. P. (2017). Latest Cretaceous climatic and environmental change in the South Atlantic region. *Paleoceanography*, *32*(5), 466–483. https://doi.org/10.1002/2016PA003007

Yao, H., Chen, X., Yin, R., Grasby, S. E., Weissert, H., Gu, X., & Wang, C. (2021). Mercury evidence of intense volcanism preceded oceanic anoxic event 1d. *Geophysical Research Letters*, *48*, e2020GL091508. https://doi.org/10.1029/2020GL091508

Zachos, J. C., Kroon, D., & Blum, P. (2004). Leg 208 Summary. *Proceedings of the Ocean Drilling Program Initial Reports* (208), 7845–9547. https://doi.org/10.2973/odp.proc.ir.208.2004

Manuscript received: June 28, 2022
Revisions required: September 15, 2022
Revised version received: December 24, 2022
Manuscript accepted: December 24, 2022

The pdf version of this paper includes an electronic supplement

Please save the electronic supplement contained in this pdf-file by clicking the blue frame above. After saving rename the file extension to .zip (for security reasons Adobe does not allow to embed .exe, .zip, .rar etc. files).

Table of contents – Electronic Supplementary Material (ESM)

Appendix A. Comparison and correlation of Holes 1262B (this work) and 1262C. Bulk $\delta^{13}C$ and $\delta^{18}O$ data in this study compared and correlated with those of Woelders et al. (2017), which are based on composite depths from several holes of Site 1262 (in the studied interval, from Holes B and C). Interval shaded in orange corresponds to the Dan-C2 interval (CIE-1 and CIE-2). Green star marks the splice tie point defined by Zachos et al. (2004). Other tie points (correlation lines) based on Dinarés-Turell et al. (2014).

Appendix B. Planktic foraminiferal distribution and indexes at Site 1262: magnetostratigraphy (Bowles 2006, Westerhold et al. 2008); planktic/benthic ratio (%); fragmentation index (FI %); relative abundance (%) of the species (index species in red); relative abundance (%) in aberrant specimens (FAI %; gray shading = increase in aberrant specimens); species richness; planktic foraminiferal zones of W11 (Wade et al. 2011) and A21 (Arenillas et al. 2021); relative abundance (%) of the genera; micro- and macroperforated taxa (%); relative abundance (%) in Cretaceous taxa; relative abundance (%) in planktic foraminiferal groups according to their depth habitat (mixed layer, thermocline and sub-thermocline dwellers); planktic foraminiferal groups: parvularugoglobigerinids s. l., biserial (*Woodringina* and *Chiloguembelina*), triserial (*Guembelitria* s. s. and *Chiloguembelitria*) and other genera (orange shading = bloom in triserial guembelitriids). Age calibration for each sample is showed, which is based on the magnetostratigraphic framework reported by Bowles (2006) and Westerhold et al. (2008) at Site 1262 (Appendix E).

Appendix C. Paleoecological preferences (depth habitats) of the planktic foraminiferal species recovered at Site 1262. References: a – Olsson et al. (1999); b – D'Hondt and Zachos (1993); c – Huber and Boersma (1994); d – Boersma and Premoli Silva (1983); e – Koutsoukos (2014); f – Huber et al. (2020); g – Berggren and Norris (1997), h – Aze et al. (2011); i – Coxall et al. (2000). See equivalence with the taxonomy of Arenillas et al. (2021) in main text and in Appendix B.

Appendix D. Geochemical data for Site 1262: bulk sediment carbon and oxygen stable isotope measurements ($\delta^{13}C_{bulk}$ and $\delta^{18}O_{bulk}$); $CaCO_3$ content (%); Hg content (ppb); Total Organic Content (TOC, %); Mn content (ppm); stratigraphic position of Hg-rich intervals (gray shading), and Dan-C2 interval (yellow shading) and its CIEs (orange shading). Age calibration for each sample is showed, which is based on the magnetostratigraphic framework reported by Bowles (2006) and Westerhold et al. (2008) at Site 1262 (Appendix E).**Appendix E.** Depth-age model for Hole 1262B, based tie points calibrated on 405 kyr eccentricity tunning (Dinarès-Turell et al. 2014, Woelders et al. 2017) but considering the lowermost Danian hiatus (see main text). The main micropaleontological and geochemical events recognized at Site 1262 are shown in depth scale (mcd), time-scale (Ma), and in kyr from the KPB. Remarks: Paleomagnetism framework for each sample follow Bowles (2006) and Westerhold et al. (2008).